TÉCNICO LISBOA

Dynamic Instability of Sandwich Panels

Rita Alves Baía dos Santos

Thesis to obtain the Master of Science Degree in

Aerospace Engineering

Supervisor: Prof. Aurélio Lima Araújo

Examination Committee

Chairperson: Prof. Afzal Suleman
Supervisor: Prof. Aurélio Lima Araújo
Member of the Committee: Prof. Filipa Andreia De Matos Moleiro

December 2022

To the 20 years old me.

We did it.

Acknowledgments

In this section I would like to thank all the people that in some way helped me, not only, during the development of this work, but also, during these crazy and rewarding last five years.

First of all, I would like to thank my supervisor, professor Aurélio Araújo for all the support, help and guiding provided during the elaboration of this work. He is an excellent professional, always available to solve any problem or doubt that arose.

Then I would like to thank the biggest investors of this journey, my family, especially my mother and father. Thank you for always supporting me and allowing me to study what I wanted with no pressures. My sister, Sara Baía, for supporting me and my crazy ideas but at the same time making sure that they aren't that crazy and I would keep my feet on the ground while making me believe that is okay to dream and have different goals.

I would like to thank my friends that always helped me to take the burden of studying at IST of my shoulders and allowed me to live less stressful and happier months (and years). Just to mention some: Ana Beatriz Macedo for always understanding, Ana Sofia for always saying yes, Iara Figueiras for all the emotional teaching, Inês Carriço for the craziness, Inês Fernandes for all the experiences, Inês Silva for the calm and discrete presence, José Nunes for teaching me so much with so little, Maria Ferreira for the memories, Mariana Henrique for the importance of second chances, Mariana Urgueira for show me what strength is, Marta Rosa for being home away from home, Rita Fardilha for the inspiration, Silviana Alves for the silence strong presence.

Last but not least, I would like to thank my colleagues, and some of them now friends, that were the firsts to be available to help me, solve my problems or answer my doubts during, not only the last six months, but, most important, during all the last five years. You showed me that we can achieve greater things when working together. I wish all the best for your future. Even though someone once said to us that they wouldn't enter a plane after we graduated I would enter any spaceship with no destination made by you!

Resumo

Placas laminadas em compósito e placas sandwich apresentam melhores propriedades quando comparadas com estruturas semelhantes. Elas são usadas para uma ampla gama de indústrias e aplicações, por esse motivo, é relevante estudar os seus comportamentos e respostas mecânicas. Habitualmente, estas estruturas estão sujeitas a diferentes tipos de cargas, tanto estáticas como dinâmicas. Assim sendo, é, também, importante estudar o seu comportamento dinâmico e melhorar o processo de design de forma a evitar o colapso das estruturas.

Neste trabalho, foram desenvolvidos, em Matlab, dois modelos para analisar placas isotrópicas, ortotrópicas e laminadas em compósito. Estes modelos têm por base a teoria de deformação de primeira ordem (FSDT) e a teoria de deformação de ordem superior (HSDT). Estas formulações são, posteriormente, usadas para modelar uma placa sandwich. Usando uma abordagem mista, o núcleo é modelado com HSDT e as faces usam FSDT. O método de elementos finitos aplicado usa elementos quadráticos de oito nós.

Uma análise de vibrações naturais foi efetuada com o intuito de validar as formulações das matrizes de massa e de rigidez. Posteriormente, foi efetuado o estudo das regiões de instabilidade dinâmica de placas isotrópicas, ortotrópicas, laminadas em compósito e sandwich. Ao longo destas análises e estudos os resultados foram validados com resultados presentes na literatura. O caso especial, de placas sandwich com núcleo viscoelástico foi, também, estudado.

Palavras-chave: Placas Sandwich, Placas Laminadas em Compósito, Instabilidade dinâmica, FSDT, HSDT

Abstract

Laminated composite plates and sandwich plates present better properties when compared to other similar structures. They are used in a wide range of industries and applications but, to do so, it is important to study their mechanical behaviour. These structures are usually under different kinds of loads, static or dynamic. For that reason it is important to study their dynamic behaviour to improve the design process and avoid failure.

In the present work two models to analyse isotropic, orthotropic and laminated composite plates were developed in Matlab. These models are based on the first-order shear deformation theory (FSDT) and the higer-order shear deformation theory (HSDT). These formulations are then used to model a sandwich plate. Using a mixed layer-wise approach, the core is modelled with the HSDT and the face sheets use the FSDT. The finite element model applies an eight-node serendipity quadratic element.

A free vibration analysis was performed in order to validate the formulation of the mass and stiffness matrices. Later on, the dynamic instability regions for isotropic, orthotropic, laminated composite and sandwich plates is studied. Through these analyses the results were validated with the ones present in the literature. A special case of sandwich plates, when the core is made of viscoelastic materials, is, also, studied.

Keywords: Sandwich Plates, Laminated Composite Plates, Dynamic Instability, FSDT, HSDT

Contents

List of Tables

List of Figures

Nomenclature

Greek symbols

$\bar{\omega}$	Non dimensional free vibration frequency
δ	Variational symbol
ϵ	Damping coefficient
γ	Shear strain
κ	Curvature
ν	Poisson's ratio
ω	Free vibration frequency
Π	Total potential energy
ρ	Density
σ	Normal stress
τ	Shear stress
θ	Frequency
$\theta_x, \theta_y, \theta_z$	Rotation of transverse normal
ε	Normal strain
ξ, η	Natural coordinates of the element

Roman symbols

$\bar{C}$	Stiffness matrix in global coordinates
$\bar{Q}$	Reduced stiffness matrix in global coordinates
A	Area
a, b	Side dimensions of the plate
C	Stiffness matrix

D	Constitutive matrix
d	Degrees of freedom
E	Young's modulus
F	Force vector
G	Shear modulus
H	Eletromechanical energy
h	Thickness
J	Jacobian
K	Linear stiffness matrix
K_G	Geometric stiffness matrix
L	Lagragian
M	Mass matrix
N	Shape functions
Q	Reduced stiffness matrix
S	Compliance matrix
T	Kinetic energy
t	Time
T_1, T_2	Rotation transformation matrix
U	Strain energy
u, v, w	Displacement field components
V	Volume domain
W	External work

Subscripts

i, j, k, l, m	Computational indexes
x, y, z	Cartesian components
0	Midplane
b	Bending
m	Membrane

s Shear

Superscripts

0 Initial

e Elementary

L Linear

NL Non linear

T Transpose

Glossary

CLPT Classical Laminated Plate Theory. xv, 11, 12, 22

CNT carbon nanotube. 4

ESL equivalent single layer. 5, 11, 50

FEM finite element method. 5, 16

FSDT first-order shear deformation theory. ix, xiii, xv, 3–5, 11, 13–17, 19, 24, 25, 33–42, 44, 50, 63

FSM finite strip method. 3

HSDT higher-order shear deformation theory. ix, xiii, xv, 4, 11, 14–17, 19, 23–25, 33–37, 39–42, 44, 45, 50, 63

LPRE leptadenia pyrotechnica rheological elastomer. 5

Chapter 1

Introduction

1.1 Motivation

Composite materials are obtained by combining two or more materials that together provide properties that are normally not achieved individually, at a reasonable cost [1]. Composite materials allow the designers and engineers to achieve element structures with the most possible appropriate characteristics for their applicability. Because of that, and even though they are complex materials that require the research of multiple scientific fields to their development, they are widely used. Composite plates are a type of composite structure. When made of layers of various materials and geometric characteristics they are called laminated plates.

A sandwich panel is a composite material consisting of two thin laminate skins and a lightweight, thick core structure. Despite the thickness of the core, sandwich composites are lightweight and have relatively high flexural strength [2]. Sandwich plates are increasingly utilised in the construction of different structures in multiple engineering applications, due to their high strength and stiffness, low weight, high durability and ease of manufacturing [3]. They are commonly used in construction of many components in automotive, aerospace, aeronautic, naval and building structures [4]. Their advantages, the development of new materials and the necessity of high performance under static, dynamic, and thermal loads guarantee that the sandwich structures will be in demand for many years [5].

(a) Aerospace[6]

(b) Shipbuilding[7]

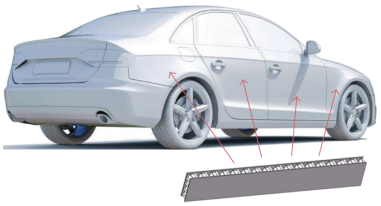

(c) Automotive[8]

Figure 1.1: Examples of composite laminate materials used in various industries

It is possible to create sandwich structures with a viscoelastic core. Usually the material used as core

is a damping material that presents great stress recovery, relaxation and creep. That means that when the applied stress is removed, some of the stresses created in the material during the recovery period are eliminated immediately and the residual stress slowly tends to zero. This technique is interesting for different aspects, such as, vibration and noise control, due to their ability to dissipate energy [9]. Since, adding this type of core on a sandwich plate changes its properties, it will affect the way that the structure reacts to different kinds of loads. For that reason it is interesting to analyse this kind of structures when studying sandwich plates. It will be possible to achieve better materials and improve the performance of the structural component. In fact, the use of this kind of materials in different industries is increasing.

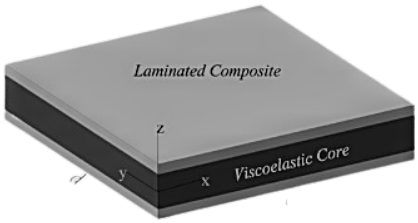

Figure 1.2: Viscoelastic Core [10]

Structural members of any engineering application are subjected to different kinds of loads and excitations. Some of these loads are static loads which permits to study the structural components behaviour with different methods in the scope of static analysis. But sometimes structures are subjected to dynamic loads, that can be periodic or not, and it is essential to study their effects on the structural behaviour. Some combination of loads can lead to dynamic instability. So it is fundamental to study the static and dynamic stability behaviour of the structural members in the design of their components [11]. Since many of these structures are made of sandwich plates, it is important to study the dynamic instability of this kind of materials in order to better understand their applicability and avoid catastrophic failures. With a better knowledge of the behaviour of as many different structures and materials as possible the better, since it will allow to do a smarter, more sustainable and safer application of materials and structures in the different industries.

1.2 State of the Art

The study of the dynamic instability on structures started long ago. At the beginning, the structures analysed were simpler than composite laminated plates or sandwich plates. Briseghella et al. [12] applied the finite element method to the definition of dynamic stability of mechanical systems previously developed by V. V. Bolotin [13]. They studied an Euler's beam and were able to achieve the Mathieu-Hill equation, which governs the dynamic stability problems, after some algebra and reasonable hypothesis.

In the last years a lot has been done in the field of dynamic stability of elastic structures. With that in mind, Mascolo [14] presented a survey of a few current research hot topics. It tries to compile the most important current events and global trends, as well as to outline any potential difficulties in the future.

Isotropic, Orthotropic and Laminated Composite Plates

For the investigation of the dynamic instability of composite laminated rectangular plates and prismatic plate structures, a B-spline finite strip method (FSM) has been developed by Wang and Dawe [15]. Their method has per base the FSDT and the set of Mathieu equations are established using Lagrange's formulation. The boundary frequencies of the instability regions are determined resorting to the method presented by Bolotin [13].

Chen et al. [16], also, based their study of the dynamic stability of laminated composite plates under arbitrary periodic loads on the FSDT. The same approach using the Bolotin's method to solve the Mathieu-Hill equations to obtain the dynamic instability boundaries was implemented.

Ramachandra and Panda [11] developed a study of the dynamic instability of composite plates under uniform, linear and parabolic dynamic in-plane loads. To start, the Ritz method was used to solve the plate membrane problem. The equations defining the plate instability boundaries are then developed utilising Hamilton's variational principle using the assessed stress distribution within the plate. The partial differential equations are converted into a set of Mathieu equations using Galerkin's approach. The boundaries of the instability region are obtained resorting, once again, to the Bolotin's method.

Loja et al. [17] proceed to a dynamic instability study of isotropic, orthotropic and composite laminated plates. Bolotin's approach was used to resolve the dynamic instability issue. Using the Rayleigh-Ritz approach, the system matrices were constructed while taking into account the use of orthogonal polynomials created for each set of boundary conditions. Before obtaining their dynamic results, they verified their model with vibration and buckling analysis. Later on, Loja and Barbosa [18] studied the free vibration and dynamic instability behaviours of a special type of composite materials, functionally graded plates, which are defined by a mixture of materials' phases that changes continually. In order to handle the problem of free vibrations, the traditional plate theory and Rayleigh-Ritz approach were considered. The Mathieu-Hill equation related to the dynamic instability problem was solved using Bolotin's approach.

Darabi and Ganesan performed a nonlinear dynamic instability analysis of laminated composite plates under both static and periodic loads. By using Galerkin's method, equations of motion with von Kármán-type nonlinearity were solved. The amplitudes of both stable and unstable solutions for steady-state vibrations, for thin plates, were obtained by applying Bolotin's approach to the governing system of nonlinear Mathieu-Hill equations [19]. Using a similar method, they also analysed the dynamic instability of internally-thickness-tapered composite plates. The non-linear von Kármán strains resulting from significant deflections and curvatures were contemplated. In order to satisfy the spatial dependence in the partial differential equation of motion and create a set of non-linear Mathieu-Hill equations, the moment-equilibrium equation of motion was then solved using the generic Galerkin method. The dynamically instability amplitudes of the steady-state vibrations were derived by using, once again, the Bolotin's approach on these equations [20].

In Ramana Reddy et al. [21] the dynamic instability regions are obtained utilising the energy approach using a single term precise trigonometric admissible function to represent the lateral deflection.

Recently, Mondal and Ramachandra [22] developed a study where they add damping to a dynamic

stability analysis of composite plates. The dynamic instability of damped laminated composite plates with embedded delaminations was investigated using a layerwise finite element model based on the B-spline function.

Sandwich Plates

A study of the free vibrations of, not only isotropic, orthotropic, laminated, but also, sandwich plates was performed by Nayak et al. [23]. They implemented two assumed strain finite element formulations of Reddy's higher-order theory.

Using a similar strategy as the majority of studies already mentioned for the isotropic, orthotropic and laminated composite plates, Kao et al. [24] analysed the dynamic instability of foam-filled sandwich plates with stiff composite laminated faces. The Galerkin approach combined with a reduced eigenfunctions transformation was used to establish the governing equations. Based on Bolotin's method, the equations of motion of the Mathieu type were constructed and utilised to identify the zones of dynamic instability. The plate theory used was the Reissner–Mindlin theory.

Applying the same method to obtain the frequencies of the boundaries of the dynamic instability regions as [24], Sankar et al. [25] studied sandwich plates with carbon nanotube (CNT) reinforced face sheets. This work, modelled the plates resorting to the FSDT and HSDT.

Sahoo and Singh [26, 27] developed two studies of the dynamic stability of laminated composite and sandwich plates. In both studies, they, also, used the Bolotin's method to obtain the dynamic instability regions. The first study is based on a modern theory, called inverse trigonometric zigzag theory. The model eliminates the requirement for a shear correction factor, resulting in transverse shear stress continuity at layer interfaces as well as traction-free boundary conditions on the plate surfaces. An effective C^0 continuous, eight noded, isoparametric element with seven field variables was used [26]. The second study is based on an inverse hyperbolic zigzag theory developed by themselves. This model, also, satisfies the interlaminar continuity conditions at the layer interfaces and the traction-free boundary conditions on the plate's surface, eliminating the need for a shear correction factor. For the standard discretization of the plate structure, a C^0 continuous isoparametric serendipity element with seven field variables was used [27].

Sandwich Plates with Viscoelastic Core

A study on free vibration of three layered sandwich plates with a viscoelastic core was performed by Permoon and Farsadi [9]. In the development of this work Lagrange's equation was used to create the governing equations of motion, which were then solved using the Rayleigh-Ritz technique. The optimal viscoelastic model was chosen for the free vibration analysis of sandwich plates after the coefficients of the fractional and classical viscoelastic models were calculated in the first stage of the analysis using the curve fitting method on existing experimental data. For fitting smooth curves to experimental data, the least squares method was used. The outcomes demonstrated that the fractional Zener model provides the best curve fit to the experimental data [9].

For the vibration and parametric instability studies of a sandwich plate with functionally graded material constraining layer, a finite element model was created by Joseph and Mohanty [28]. The top and bottom layer displacements were thought of as being linear functions of the lateral and transverse displacements of the viscoelastic core layer. The FSDT was employed to account for the transverse shear of the face layers, and in addition to shear deformation of the core, the analysis also took into account the impacts of transverse and longitudinal deformations. This model is able to be applied to plates with thick and thin core layer.

Ojha and Dwivedy [29] performed an analysis on a three-layered sandwich plate with a viscoelastic core made of leptadenia pyrotechnica rheological elastomer (LPRE). A parametrically stimulated system was used in the finite element method (FEM) to generate the governing equation of motion. The sandwich plate's instability zones were discovered utilising the modified Hsu approach. Experimental results were used to estimate the newly created LPRE core's shear storage modulus and loss modulus.

It is relevant to mention that sandwich plates can be modelled using different methods. From the works presented it is possible to conclude that most of them resorted to equivalent single layer (ESL) theories. These theories do not take into account the transverse compressibility into the core during the dynamic analysis. To overcome that problem, layer-wise theories of sandwich plates have been developed. For instance, Li [30] worked in a layer-wise theory for laminated composite structures, including sandwich plates, and Moreira and Rodrigues [31] proposed a layerwise theory for sandwich plates with thin soft core. Layerwise theories, a quasi-3-dimensional technique, is becoming more and more popular since it is more accurate than most ESL theories and computationally less expensive than 3D-based displacement FEMs [30]. However, layer-wise theories demand that the unknown displacement components be taken at every layer interface, which means that the formulation's number of unknowns grows as the number of layers does, necessitating a significant amount of computational work. With the dynamic instability analyses, also, requiring some computational effort, literature becomes quite scarce when dealing with layer-wise theories in sandwich plates to analyse their dynamic instability.

1.3 Objectives, Deliverables and Additional Notes

This work is derived as an extension of Tomé [32]. Actually, the finite element models to be used and developed in this work are based on the models developed by Araújo et al. [33] for dynamic analysis and extended to buckling analysis by Tomé [32]. Tomé [32] presents a static and buckling analysis of isotropic, orthotopric, laminated and sandwich plates using a finite element model written in Matlab. In fact, this work uses as base Tomé's [32] Matlab formulations. These are adapted and developed in order to achieve the goals of the present work.

With that said, the objective of the present work is to perform a new analysis, a dynamic analysis, to isotropic, orthotropic, laminated and sandwich plates. The dynamic analysis should be able to provide the regions of dynamic instability. In order to perform the dynamic analysis this work needs to build the mass matrix of the systems studied and add it to the matrices already formulated by Tomé [32]. For the sake of improving the reliability of the results presented, a vibration analysis is performed to compare

the results obtained for the natural frequencies to the theoretical values and then, possibly, validate the formulation of the mass matrix.

This work also intends to do a dynamic analysis and obtain the regions of instability of sandwich plates with viscoelastic cores. At the end, it aims to be able to draw conclusions about the dynamic instability of the different composite structures studied.

1.4 Thesis Outline

This work presents 5 chapters. The first one is dedicated to the introduction. This chapter includes the motivation behind the study of sandwich plates and their dynamic behaviour, followed by the state of the art and its objectives and deliverables. In the state of art section a review of the work developed before in the dynamic instability analysis of isotropic, orthotropic, laminated composite and sandwich plates is presented. At last, the expected goals for the scope of this work are stated.

Chapter 2, presents the multiple models used to formulate the structures under study, including the finite element model and the laminate theories. A vibration analysis in order to validate part of the models presented is performed on isotropic and orthotropic plates.

The dynamic analysis is covered in Chapter 3. The numerical model used to compute the results is presented. Once the analysis is done, the results obtained to the different structures analysed are displayed and studied.

In Chapter 4, the models presented in Chapter 2 are combined in order to formulate a model that can translate the behaviour of sandwich plates. A vibration analysis is also performed in these structures to validate the model. The model developed in Chapter 3 is applied to these plates and a dynamic stability analysis is performed. Subsequently, a viscoelastic core is added to the sandwich plate. The adaptions needed to be done to the model used before are also presented. Afterwards, a dynamic stability analysis is performed to the new structure and the results are presented and studied.

Finally, the last chapter covers the conclusions, where the achievements of this work are reviewed. In addition, some guidelines for future works regarding the study of both sandwich plates and dynamic analysis are given.

Chapter 2

Development of Plate Elements

In this chapter the finite element models used to formulate the different structures that are going to be studied in this work is presented.

First, two different finite element models for laminated composited plates, based on two different laminated theories, are presented. A vibration analysis is conducted in order to obtain the fundamental natural frequency. The results are then compared to the ones found in the literature to validate the models presented.

2.1 Laminated Composite Plates

A laminate is an assembly of more than one lamina stacked in order to obtain a structure with the desired thickness and stiffness, in which a lamina or ply is a sheet of composite material.

The layers used to build a laminate are usually fiber-reinforced laminae, which consist in many fibers embedded in a matrix material. The type of fiber used will affect the properties of the material, and those properties will also be direction-dependent. Then they need to be studied and produced having in the mind the load directions they will be under. To increase toughness coupling agents can be added as well as fillers that will improve the bonding between the fibers and the matrix material.

On the other hand, to achieve the desired structural stiffness and strength, plies can be stacked into laminated composites in a way to combine the best aspects of the constituent layers. This process is called lamination. The majority of laminated composites consist of unidirectional fiber-reinforced laminae, which can be stacked in a way that each lamina is oriented in the same or different directions. The term lamination scheme or stacking sequence consists on the sequence of various orientations of a fiber-reinforced composite layer in a laminate. A representation of lamination can be seen in Figure 2.1.

So, one of the advantages of composite materials is the possibility to structure and orient layers in a certain sequence. This advantage becomes really important when it is possible to match the layers orientation with the applied load, presenting better mechanical reactions to that load.

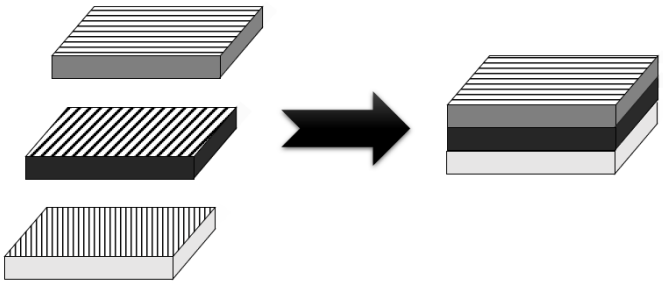

Figure 2.1: Laminate with plies with different directions

2.1.1 Constitutive Equation of a Lamina

In this section the formulations used to study a lamina will be presented. These formulations will be, later, put together to formulate models that enable the study of laminated plates.

To formulate the constitutive equation of a lamina it is assumed that [34]:

1. a lamina is a continuum;

2. a lamina behaves as a linear elastic material.

The first assumption comes from considering the macromechanical behaviour of a lamina. On the other hand, the second assumption implies that the generalised Hooke's law is valid. The generalised Hooke's law for an anisotropic material under isothermal condition, in a contracted notation, is written as:

$$\sigma_i = C_{ij}\varepsilon_j \tag{2.1}$$

where σ_i are the stress components, ε_j are the strain components and C_{ij} are the material coefficients, all referred to an orthogonal Cartesian coordinate system (x_1, x_2, x_3) fixed in the body, Figure 2.2.

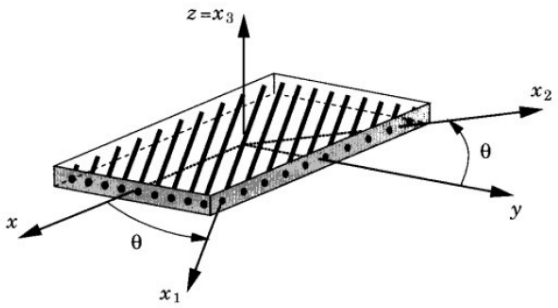

Figure 2.2: Coordinate system of a laminate composite ply [34]

In the case that one wants to develop micromechanical constitutive models for inelastic behaviour of a lamina, both assumptions can be removed. From a macromechanical point of view, a composite lamina behaves as an orthotropic material.

Orthotropic Plate

An orthotropic material has three mutually orthogonal planes of material symmetry.

If the coordinate planes are chosen parallel to the three orthogonal planes of symmetry, that is, the principal material directions (x_1, x_2), the stress-strain relations can be given by:

$$\begin{Bmatrix} \sigma_{11} \\ \sigma_{22} \\ \sigma_{33} \\ \sigma_{23} \\ \sigma_{13} \\ \sigma_{12} \end{Bmatrix} = \begin{bmatrix} C_{11} & C_{12} & C_{13} & 0 & 0 & 0 \\ C_{21} & C_{22} & C_{23} & 0 & 0 & 0 \\ C_{31} & C_{32} & C_{33} & 0 & 0 & 0 \\ 0 & 0 & 0 & C_{44} & 0 & 0 \\ 0 & 0 & 0 & 0 & C_{55} & 0 \\ 0 & 0 & 0 & 0 & 0 & C_{66} \end{bmatrix} \begin{Bmatrix} \varepsilon_{11} \\ \varepsilon_{22} \\ \varepsilon_{33} \\ \varepsilon_{23} \\ \varepsilon_{13} \\ \varepsilon_{12} \end{Bmatrix} = \begin{bmatrix} \frac{1}{E_1} & -\frac{\nu_{21}}{E_2} & -\frac{\nu_{31}}{E_3} & 0 & 0 & 0 \\ -\frac{\nu_{12}}{E_1} & \frac{1}{E_2} & -\frac{\nu_{32}}{E_3} & 0 & 0 & 0 \\ -\frac{\nu_{13}}{E_1} & -\frac{\nu_{23}}{E_2} & \frac{1}{E_3} & 0 & 0 & 0 \\ 0 & 0 & 0 & \frac{1}{G_{23}} & 0 & 0 \\ 0 & 0 & 0 & 0 & \frac{1}{G_{13}} & 0 \\ 0 & 0 & 0 & 0 & 0 & \frac{1}{G_{12}} \end{bmatrix}^{-1} \begin{Bmatrix} \varepsilon_{11} \\ \varepsilon_{22} \\ \varepsilon_{33} \\ \varepsilon_{23} \\ \varepsilon_{13} \\ \varepsilon_{12} \end{Bmatrix} \tag{2.2}$$

where $[C]$ is the stiffness matrix in the principal directions (x_1, x_2), which is the inverse of the compliance matrix $[S]$.

The global stress-strain relations can be written as:

$$\begin{Bmatrix} \sigma_{xx} \\ \sigma_{yy} \\ \sigma_{zz} \\ \sigma_{yz} \\ \sigma_{xz} \\ \sigma_{zy} \end{Bmatrix} = \begin{bmatrix} \bar{C}_{11} & \bar{C}_{12} & \bar{C}_{13} & 0 & 0 & \bar{C}_{16} \\ \bar{C}_{21} & \bar{C}_{22} & \bar{C}_{23} & 0 & 0 & \bar{C}_{26} \\ \bar{C}_{31} & \bar{C}_{32} & \bar{C}_{33} & 0 & 0 & \bar{C}_{36} \\ 0 & 0 & 0 & \bar{C}_{44} & \bar{C}_{45} & 0 \\ 0 & 0 & 0 & \bar{C}_{54} & \bar{C}_{55} & 0 \\ \bar{C}_{61} & \bar{C}_{62} & \bar{C}_{63} & 0 & 0 & \bar{C}_{66} \end{bmatrix} \begin{Bmatrix} \varepsilon_{xx} \\ \varepsilon_{yy} \\ \varepsilon_{zz} \\ 2\varepsilon_{yz} \\ 2\varepsilon_{xz} \\ 2\varepsilon_{xy} \end{Bmatrix} \tag{2.3}$$

where $\bar{C}_{ij}$ are the transformed elastic coefficients in global coordinates and can be obtained by:

$$\left[\bar{C}\right] = [T_1]\,[C]\,[T_1]^T \tag{2.4}$$

where $\left[\bar{C}\right]$ is the elastic stiffness matrix in the coordinates (x, y, z) and $[T_1]$ is the rotation transformation matrix that can be written as:

$$\left[T_1\right] = \begin{bmatrix} \cos^2\theta & \sin^2\theta & 0 & 0 & 0 & -2\sin\theta\cos\theta \\ \sin^2\theta & \cos^2\theta & 0 & 0 & 0 & 2\sin\theta\cos\theta \\ 0 & 0 & 1 & 0 & 0 & 0 \\ 0 & 0 & \cos\theta & \sin\theta & 0 & 0 \\ 0 & 0 & -\sin\theta & \cos\theta & 0 & 0 \\ \sin\theta\cos\theta & -\sin\theta\cos\theta & 0 & 0 & 0 & \cos^2\theta - \sin^2\theta \end{bmatrix} \tag{2.5}$$

During the analysis of laminated composites materials it is generally possible to consider $\sigma_{33} = 0$, as in a plane stress-reduced state. According to this hypothesis, the constitutive equations in the principal directions (x_1, x_2) can be given by:

$$\begin{Bmatrix}\sigma_{11}\\ \sigma_{22}\\ \sigma_{23}\\ \sigma_{13}\\ \sigma_{12}\end{Bmatrix} = \begin{bmatrix}Q_{11} & Q_{12} & 0 & 0 & 0\\ Q_{21} & Q_{22} & 0 & 0 & 0\\ 0 & 0 & Q_{44} & 0 & 0\\ 0 & 0 & 0 & Q_{55} & 0\\ 0 & 0 & 0 & 0 & Q_{66}\end{bmatrix} \begin{Bmatrix}\varepsilon_{11}\\ \varepsilon_{22}\\ \varepsilon_{23}\\ \varepsilon_{13}\\ \varepsilon_{12}\end{Bmatrix} = \begin{bmatrix}\frac{E_1}{1-\nu_{12}\nu_{21}} & \frac{E_1\nu_{21}}{1-\nu_{12}\nu_{21}} & 0 & 0 & 0\\ \frac{E_1\nu_{21}}{1-\nu_{12}\nu_{21}} & \frac{E_2}{1-\nu_{12}\nu_{21}} & 0 & 0 & 0\\ 0 & 0 & G_{23} & 0 & 0\\ 0 & 0 & 0 & G_{13} & 0\\ 0 & 0 & 0 & 0 & G_{12}\end{bmatrix} \begin{Bmatrix}\varepsilon_{11}\\ \varepsilon_{22}\\ \varepsilon_{23}\\ \varepsilon_{13}\\ \varepsilon_{12}\end{Bmatrix} \tag{2.6}$$

where Q_{ij} are the components of the plane stress-reduced stiffness.

The plane stress-reduced constitutive equations in global coordinates (x, y) can be written as:

$$\begin{Bmatrix}\sigma_{xx}\\ \sigma_{yy}\\ \sigma_{yz}\\ \sigma_{xz}\\ \sigma_{xy}\end{Bmatrix} = \begin{bmatrix}\bar{Q}_{11} & \bar{Q}_{12} & 0 & 0 & 0\\ \bar{Q}_{21} & \bar{Q}_{22} & 0 & 0 & 0\\ 0 & 0 & \bar{Q}_{44} & 0 & 0\\ 0 & 0 & 0 & \bar{Q}_{55} & 0\\ 0 & 0 & 0 & 0 & \bar{Q}_{66}\end{bmatrix} \begin{Bmatrix}\varepsilon_{xx}\\ \varepsilon_{yy}\\ \varepsilon_{yz}\\ \varepsilon_{xz}\\ \varepsilon_{xy}\end{Bmatrix} \tag{2.7}$$

In this case, $\left[\bar{Q}\right]$, which is the reduced stiffness matrix in global coordinates (x, y) can be given by:

$$\left[\bar{Q}\right] = \left[T_2\right]\left[Q\right]\left[T_2\right]^T \tag{2.8}$$

where $[T_2]$ is the rotation transformation matrix for the stress-reduce state and can be written as:

$$\left[T_2\right] = \begin{bmatrix}\cos^2\theta & \sin^2\theta & 0 & 0 & -2\sin\theta\cos\theta\\ \sin^2\theta & \cos^2\theta & 0 & 0 & 2\sin\theta\cos\theta\\ 0 & 0 & \cos\theta & \sin\theta & 0\\ 0 & 0 & -\sin\theta & \cos\theta & 0\\ \sin\theta\cos\theta & -\sin\theta\cos\theta & 0 & 0 & \cos^2\theta - \sin^2\theta\end{bmatrix} \tag{2.9}$$

Isotropic Plate

An isotropic material presents an infinite number of planes of material symmetry, which means that each material property is independent of the direction. This can be mathematically translated into:

$$E = E_1 = E_2 = E_3 \tag{2.10a}$$

$$\nu = \nu_{12} = \nu_{13} = \nu_{23} \tag{2.10b}$$

$$G = G_{12} = G_{13} = G_{23} \tag{2.10c}$$

And these properties are related as follows:

$$G = \frac{E}{2\left(1+\nu\right)} \tag{2.11}$$

So, the stress-strain relations for an isotropic material are obtained by:

$$\begin{Bmatrix} \sigma_{11} \\ \sigma_{22} \\ \sigma_{33} \\ \sigma_{23} \\ \sigma_{13} \\ \sigma_{12} \end{Bmatrix} = \begin{bmatrix} C_{11} & C_{12} & C_{12} & 0 & 0 & 0 \\ C_{12} & C_{11} & C_{12} & 0 & 0 & 0 \\ C_{12} & C_{12} & C_{11} & 0 & 0 & 0 \\ 0 & 0 & 0 & C & 0 & 0 \\ 0 & 0 & 0 & 0 & C & 0 \\ 0 & 0 & 0 & 0 & 0 & C \end{bmatrix} \begin{Bmatrix} \varepsilon_{11} \\ \varepsilon_{22} \\ \varepsilon_{33} \\ \varepsilon_{23} \\ \varepsilon_{13} \\ \varepsilon_{12} \end{Bmatrix} \tag{2.12}$$

where $C = (C_{11} - C_{12})/2$.

2.2 Laminated Plate Theories

Since composite laminates present planar dimensions up to two orders of magnitude larger than their thickness, and can be used in applications that require membrane and bending strengths they can be treated as plate elements. Therefore there are plenty of different approaches to describe the behaviour of composite plates. The ones used in this work are ESL plate theories. These theories reduce a 3D problem to a 2D problem by making suitable assumptions regarding the kinematics of deformation or the stress state through the thickness. This allows to reduce the computational effort and the complexity of the problem without losing relevant accuracy. This happens because by taking into account the Cartesian coordinate system at the mid-surface of the entire structure, models based on similar single layer plate theories are created, and the deformation of the plate is described in terms of the characteristics of this reference plane. Because of this, the overall number of degrees of freedom is independent of the number of plies.

The ESL theories consider the form of the displacement field or stress field as a linear combination of unknown functions and the thickness coordinate, which can be mathematically translated into [34]:

$$\varphi_i(x, y, z, t) = \sum_{j=0}^{N} (z)^j \varphi_i^j(x, y, t) \tag{2.13}$$

where φ_i is the ith component of displacement or stress, t denotes the time, (x, y) the in-plane coordinates, z is the thickness and φ_i^j are the functions to be determined. For φ_i being the displacements, the equations governing φ_i^j are given by the principle of virtual displacements:

$$0 = \int_0^T (\delta U + \delta V - \delta K)\, dt \tag{2.14}$$

The CLPT, the FSDT and the HSDT are some ESL theories that are already well developed and studied presenting good results. The three theories will be presented, but only the FSDT and HSDT will be more detailed, since they are the ones that will be applied to develop the models used to study the structures analysed in this work.

2.2.1 Classical Laminate Plate Theory (CLPT)

In the classical laminate plate theory the following assumptions are made [34]:

1. Straight lines perpendicular to the midsurface (i.e., transverse normals) before deformation remain straight after deformation.
2. The transverse normals do not experience elongation (i.e., they are inextensible, $\varepsilon_{zz} = 0$).
3. The transverse normals rotate such that they remain perpendicular to the midsurface after deformation.

A visual representation of these assumptions can be seen in Figure 2.3.

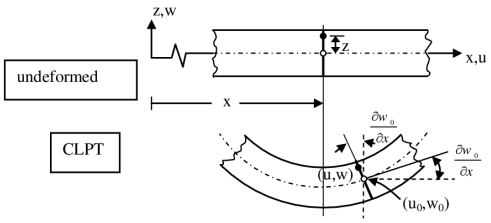

Figure 2.3: Deformation of a transverse normal according to the CLPT [34]

In the CLPT the displacement field is given by:

$$u\left(x,y,z,t\right) = u_0\left(x,y,t\right) - z\frac{\partial w_0}{\partial x} \tag{2.15a}$$

$$v\left(x,y,z,t\right) = v_0\left(x,y,t\right) - z\frac{\partial w_0}{\partial y} \tag{2.15b}$$

$$w\left(x,y,z,t\right) = w_0\left(x,y,t\right) \tag{2.15c}$$

where u, v and w are the components of the resultant displacement field and (u_0, v_0, w_0) are the displacements of a material point $(x, y, 0)$ in (x, y, z) coordinate directions.

Since this theory is not used in the present work to develop the models for the structures studied, it will not be presented more detailed information regarding it.

2.2.2 First-Order Shear Deformation Theory (FSDT)

For the first-order shear deformation theory the last assumption made for the previous theory is relaxed. Then the assumptions used in this theory are the following:

1. Straight lines perpendicular to the midsurface (i.e., transverse normals) before deformation remain straight after deformation.
2. The transverse normals do not experience elongation, this means that they are inextensible.

A visual representation of the impact of these assumptions on the deformation of a transverse normal can be seen in Figure 2.4.

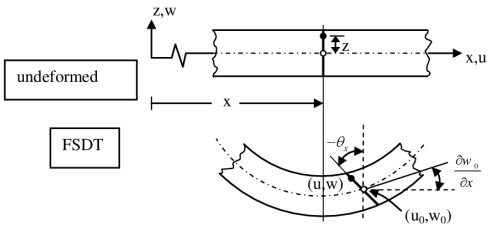

Figure 2.4: Deformation of a transverse normal according to the FSDT [35]

Regarding the displacement field, the FSDT considers:

$$u\left(x,y,z,t\right) = u_0\left(x,y,t\right) + z\theta_x\left(x,y,t\right) \tag{2.16a}$$

$$v\left(x,y,z,t\right) = v_0\left(x,y,t\right) + z\theta_y\left(x,y,t\right) \tag{2.16b}$$

$$w\left(x,y,z,t\right) = w_0\left(x,y,t\right) \tag{2.16c}$$

where θ_x and θ_y are the rotation of a transverse normal about the y and x axis, respectively.

The linear and non linear strain-displacement relations are given by:

$$\varepsilon = \varepsilon^L + \varepsilon^{NL} \tag{2.17}$$

Where the ε^L are given by:

$$\begin{aligned}
\varepsilon^L_{xx} &= \frac{\partial u}{\partial x} \\
\varepsilon^L_{yy} &= \frac{\partial v}{\partial y} \\
\varepsilon^L_{zz} &= \frac{\partial w}{\partial z} \\
\varepsilon^L_{xy} &= \frac{1}{2}\left[\frac{\partial u}{\partial y} + \frac{\partial w}{\partial x}\right] \\
\varepsilon^L_{yz} &= \frac{1}{2}\left[\frac{\partial v}{\partial z} + \frac{\partial w}{\partial y}\right] \\
\varepsilon^L_{xz} &= \frac{1}{2}\left[\frac{\partial u}{\partial z} + \frac{\partial v}{\partial x}\right]
\end{aligned} \tag{2.18}$$

And ε^{NL} are given by:

$$\begin{aligned}
\varepsilon^{NL}_{xx} &= \frac{1}{2}\left[\left(\frac{\partial u}{\partial x}\right)^2 + \left(\frac{\partial v}{\partial x}\right)^2 + \left(\frac{\partial w}{\partial x}\right)^2\right] \\
\varepsilon^{NL}_{yy} &= \frac{1}{2}\left[\left(\frac{\partial u}{\partial y}\right)^2 + \left(\frac{\partial v}{\partial y}\right)^2 + \left(\frac{\partial w}{\partial y}\right)^2\right] \\
\varepsilon^{NL}_{zz} &= \frac{1}{2}\left[\left(\frac{\partial u}{\partial z}\right)^2 + \left(\frac{\partial v}{\partial z}\right)^2 + \left(\frac{\partial w}{\partial z}\right)^2\right] \\
\varepsilon^{NL}_{xy} &= \frac{1}{2}\left[\frac{\partial u}{\partial x}\frac{\partial u}{\partial y} + \frac{\partial v}{\partial x}\frac{\partial v}{\partial y} + \frac{\partial w}{\partial x}\frac{\partial w}{\partial y}\right] \\
\varepsilon^{NL}_{yz} &= \frac{1}{2}\left[\frac{\partial u}{\partial y}\frac{\partial u}{\partial z} + \frac{\partial v}{\partial y}\frac{\partial v}{\partial z} + \frac{\partial w}{\partial y}\frac{\partial w}{\partial z}\right] \\
\varepsilon^{NL}_{xz} &= \frac{1}{2}\left[\frac{\partial u}{\partial x}\frac{\partial u}{\partial z} + \frac{\partial v}{\partial x}\frac{\partial v}{\partial z} + \frac{\partial w}{\partial x}\frac{\partial w}{\partial z}\right]
\end{aligned} \tag{2.19}$$

Substituting equations (2.16) into equation (2.18), the non zero linear strain terms are given by:

$$\begin{array}{lll} \varepsilon_{xx}^{L} & = \frac{\partial u_0}{\partial x} + z\frac{\partial \theta_x}{\partial x} & = \varepsilon_{xx}^{(0)} + z\kappa_{xx}^{(1)} \\ \varepsilon_{yy}^{L} & = \frac{\partial v_0}{\partial y} + z\frac{\partial \theta_y}{\partial y} & = \varepsilon_{yy}^{(0)} + z\kappa_{yy}^{(1)} \\ \gamma_{xy}^{L} & = \frac{\partial u_0}{\partial y}\frac{\partial v_0}{\partial x} + z\left(\frac{\partial \theta_x}{\partial y} + \frac{\partial \theta_y}{\partial x}\right) & = \gamma_{xy}^{(0)} + z\kappa_{xy}^{(1)} \\ \gamma_{yz}^{L} & = \theta_y + \frac{\partial w_0}{\partial y} & = \gamma_{yz}^{(0)} \\ \gamma_{xz}^{L} & = \theta_x + \frac{\partial w_0}{\partial x} & = \gamma_{xz}^{(0)} \end{array} \tag{2.20}$$

where $\varepsilon_{xx}^{(0)}$, $\varepsilon_{yy}^{(0)}$, $\gamma_{xy}^{(0)}$, $\gamma_{xz}^{(0)}$ and $\gamma_{yz}^{(0)}$ represent the mid-surface strains and $\kappa_{xx}^{(1)}$, $\kappa_{yy}^{(1)}$ and $\kappa_{xy}^{(1)}$ are the curvatures. The following vectors group these variables regarding their contribution to membrane (m), coupling (c), bending (b) and shear (s).

$$\{\varepsilon_m\} = \begin{Bmatrix} \varepsilon_{xx}^{(0)} \\ \varepsilon_{yy}^{(0)} \\ \gamma_{xy}^{(0)} \end{Bmatrix}, \qquad \{\varepsilon_b\} = \begin{Bmatrix} \kappa_{xx}^{(1)} \\ \kappa_{yy}^{(1)} \\ \kappa_{xy}^{(1)} \end{Bmatrix} \qquad \{\varepsilon_s\} = \begin{Bmatrix} \gamma_{yz}^{(0)} \\ \gamma_{xz}^{(0)} \end{Bmatrix}, \tag{2.21}$$

The constitutive matrix of the laminate $[D]$ is given by:

$$[D] = \begin{bmatrix} [D_m] & [D_c] & 0 \\ [D_c] & [D_b] & 0 \\ 0 & 0 & [D_s] \end{bmatrix} \tag{2.22}$$

In the FSDT the matrices $[D_m]$, $[D_c]$, $[D_b]$ and $[D_s]$ are obtained by:

$$[D_m] = \sum_{k=1}^{NL} \bar{Q}_{ij}^{(k)} H_1, \qquad [D_c] = \sum_{k=1}^{NL} \bar{Q}_{ij}^{(k)} H_2, \qquad [D_b] = \sum_{k=1}^{NL} \bar{Q}_{ij}^{(k)} H_3, \qquad [D_s] = \sum_{k=1}^{NL} \bar{Q}_{lm}^{(k)} H_1 \tag{2.23}$$

where NL is the number of layers of the composite laminated plate, $i, j \in \{1, 2, 6\}$, $l, m \in \{4, 5\}$ and H is given by:

$$H_n = \frac{1}{n}\left(z_k^n - z_{k+1}^n\right) \tag{2.24}$$

2.2.3 Higher-Order Shear Deformation Theory (HSDT)

The higher-order shear deformation theory also relaxes the last two assumptions. The loosening of the kinematic hypothesis makes it possible that straight normals to the middle plane before deformation may become curves after deformation.

A visual representation of the HSDT can be seen in Figure 2.5.

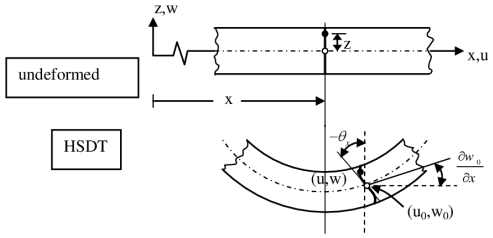

Figure 2.5: Deformation of a transverse normal according to the HSDT [35]

For the HSDT the displacement field is written as:

$$u\left(x,y,z,t\right)=u_0\left(x,y,t\right)+z\theta_x\left(x,y,t\right)+z^2u_0^*\left(x,y,t\right)+z^3\theta_x^*\left(x,y,t\right) \tag{2.25a}$$

$$v\left(x,y,z,t\right)=v_0\left(x,y,t\right)+z\theta_y\left(x,y,t\right)+z^2v_0^*\left(x,y,t\right)+z^3\theta_y^*\left(x,y,t\right) \tag{2.25b}$$

$$w\left(x,y,z,t\right)=w_0\left(x,y,t\right)+z\theta_z\left(x,y,t\right)+z^2w_0^*\left(x,y,t\right) \tag{2.25c}$$

where u_0^*, v_0^*, w_0^*, θ_x^*, θ_y^* and θ_z are higher order terms in the series expansion to be determined.

Doing the same that was done for FSDT, and substituting equation (2.25) into equation (2.18), the linear strain terms associated with HSDT are written as:

$$\varepsilon_{xx}^L=\frac{\partial u_0}{\partial x}+z\frac{\partial\theta_x}{\partial x}+z^2\frac{\partial u_0^*}{\partial x}+z^3\frac{\partial\theta_x^*}{\partial x}=\varepsilon_{xx}^{(0)}+z\kappa_{xx}^{(1)}+z^2\varepsilon_{xx}^{(2)}+z^3\kappa_{xx}^{(3)} \tag{2.26a}$$

$$\varepsilon_{yy}^L=\frac{\partial v_0}{\partial y}+z\frac{\partial\theta_y}{\partial y}+z^2\frac{\partial v_0^*}{\partial y}+z^3\frac{\partial\theta_y^*}{\partial y}=\varepsilon_{yy}^{(0)}+z\kappa_{yy}^{(1)}+z^2\varepsilon_{yy}^{(2)}+z^3\kappa_{yy}^{(3)} \tag{2.26b}$$

$$\varepsilon_{zz}^L=\theta_z+z2w_0^*=\varepsilon_{zz}^{(0)}+z\kappa_{zz}^{(1)} \tag{2.26c}$$

$$\gamma_{yz}^L=\left(\theta_y+\frac{\partial w_0}{\partial y}\right)+z\left(2v_0^*+\frac{\partial\theta_z}{\partial y}\right)+z^2\left(3\theta_y^*+\frac{\partial w_0^*}{\partial y}\right)=\gamma_{yz}^{(0)}+z\kappa_{yz}^{(1)}+z^2\gamma_{yz}^{(2)} \tag{2.26d}$$

$$\gamma_{xz}^L=\left(\theta_x+\frac{\partial w_0}{\partial x}\right)+z\left(2u_0^*+\frac{\partial\theta_z}{\partial x}\right)+z^2\left(3\theta_x^*+\frac{\partial w_0^*}{\partial x}\right)=\gamma_{xz}^{(0)}+z\kappa_{xz}^{(1)}+z^2\gamma_{xz}^{(2)} \tag{2.26e}$$

$$\gamma_{xy}^L=\left(\frac{\partial u_0}{\partial y}+\frac{\partial v_0}{\partial x}\right)+z\left(\frac{\partial\theta_x}{\partial y}+\frac{\partial\theta_y}{\partial x}\right)+z^2\left(\frac{\partial u_0^*}{\partial y}+\frac{\partial v_0^*}{\partial x}\right)+z^3\left(\frac{\partial\theta_x^*}{\partial y}+\frac{\partial\theta_y^*}{\partial x}\right)= \\ =\gamma_{xy}^{(0)}+z\kappa_{xy}^{(1)}+z^2\gamma_{xy}^{(2)}+z^3\kappa_{xy}^{(3)} \tag{2.26f}$$

where $\varepsilon_{xx}^{(0)}$, $\varepsilon_{yy}^{(0)}$, $\varepsilon_{zz}^{(0)}$, $\gamma_{xy}^{(0)}$, $\gamma_{xz}^{(0)}$ and $\gamma_{yz}^{(0)}$ represent the mid-surface strains, $\kappa_{xx}^{(1)}$, $\kappa_{yy}^{(1)}$, $\kappa_{zz}^{(1)}$, $\kappa_{xy}^{(1)}$, $\kappa_{xz}^{(1)}$ and $\kappa_{yz}^{(1)}$ describe the curvatures associated with the first order terms in the series expansion, $\varepsilon_{xx}^{(2)}$, $\varepsilon_{yy}^{(2)}$, $\gamma_{xy}^{(2)}$, $\gamma_{xz}^{(2)}$ and $\gamma_{yz}^{(2)}$ are the mid-surface strains associated with the second order terms and $\kappa_{xx}^{(3)}$, $\kappa_{yy}^{(3)}$ and $\kappa_{xy}^{(3)}$ describe the curvatures associated with the third order terms. The following vectors group these variables regarding their contribution to membrane (m), bending (b) and shear (s).

$$\{\varepsilon_m\} = \begin{Bmatrix} \varepsilon_{xx}^{(0)} \\ \varepsilon_{yy}^{(0)} \\ \gamma_{xy}^{(0)} \\ \varepsilon_{xx}^{(2)} \\ \varepsilon_{yy}^{(2)} \\ \gamma_{xy}^{(2)} \\ \varepsilon_{zz}^{(0)} \end{Bmatrix}, \qquad \{\varepsilon_b\} = \begin{Bmatrix} \kappa_{xx}^{(1)} \\ \kappa_{yy}^{(1)} \\ \kappa_{xy}^{(1)} \\ \kappa_{xx}^{(3)} \\ \kappa_{yy}^{(3)} \\ \kappa_{xy}^{(3)} \\ \kappa_{zz}^{(1)} \end{Bmatrix} \qquad \{\varepsilon_s\} = \begin{Bmatrix} \gamma_{yz}^{(0)} \\ \gamma_{xz}^{(0)} \\ \gamma_{yz}^{(2)} \\ \gamma_{xz}^{(2)} \\ \kappa_{yz}^{(1)} \\ \kappa_{xz}^{(1)} \end{Bmatrix}, \tag{2.27}$$

In the HSDT the matrices $[D_m]$, $[D_c]$, $[D_b]$ and $[D_s]$, used to obtain the constitutive matrix of the laminate $[D]$ as shown in equation (2.22), are given by:

$$[D_m] = \sum_{k=1}^{NL} \begin{bmatrix} \bar{C}_{ij}^{(k)} H_1 & \bar{C}_{ij}^{(k)} H_3 & \bar{C}_{i3}^{(k)} H_1 \\ \bar{C}_{ij}^{(k)} H_3 & \bar{C}_{ij}^{(k)} H_5 & \bar{C}_{i3}^{(k)} H_3 \\ \bar{C}_{3j}^{(k)} H_1 & \bar{C}_{3j}^{(k)} H_3 & \bar{C}_{33}^{(k)} H_1 \end{bmatrix} \tag{2.28a}$$

$$[D_c] = \sum_{k=1}^{NL} \begin{bmatrix} \bar{C}_{ij}^{(k)} H_2 & \bar{C}_{ij}^{(k)} H_4 & \bar{C}_{i3}^{(k)} H_2 \\ \bar{C}_{ij}^{(k)} H_4 & \bar{C}_{ij}^{(k)} H_6 & \bar{C}_{i3}^{(k)} H_4 \\ \bar{C}_{3j}^{(k)} H_2 & \bar{C}_{3j}^{(k)} H_4 & \bar{C}_{33}^{(k)} H_2 \end{bmatrix} \tag{2.28c}$$

$$[D_b] = \sum_{k=1}^{NL} \begin{bmatrix} \bar{C}_{ij}^{(k)} H_3 & \bar{C}_{ij}^{(k)} H_5 & \bar{C}_{i3}^{(k)} H_3 \\ \bar{C}_{ij}^{(k)} H_5 & \bar{C}_{ij}^{(k)} H_7 & \bar{C}_{i3}^{(k)} H_5 \\ \bar{C}_{3j}^{(k)} H_3 & \bar{C}_{3j}^{(k)} H_5 & \bar{C}_{33}^{(k)} H_3 \end{bmatrix} \tag{2.28b}$$

$$[D_s] = \sum_{k=1}^{NL} \begin{bmatrix} \bar{C}_{lm}^{(k)} H_1 & \bar{C}_{lm}^{(k)} H_3 & \bar{C}_{lm}^{(k)} H_2 \\ \bar{C}_{lm}^{(k)} H_3 & \bar{C}_{lm}^{(k)} H_5 & \bar{C}_{lm}^{(k)} H_4 \\ \bar{C}_{lm}^{(k)} H_2 & \bar{C}_{lm}^{(k)} H_4 & \bar{C}_{lm}^{(k)} H_3 \end{bmatrix} \tag{2.28d}$$

where NL is the number of layers, $i, j \in \{1, 2, 6\}$, $l, m \in \{4, 5\}$ and H is obtained as shown in equation (2.24).

2.3 Finite Element Model

In this section the Finite Element Model (FEM) used to model the plates is presented. It is important to mention that two FEMs are developed, since this work focus on two laminated plate theories. So, one finite element model is based on the FSDT and the other on the HSDT. The models presented use an eight-node serendipity quadratic element, whose representation can be seen on Figure 2.6. Each node has 5 and 11 degrees of freedom for the FSDT and HSDT, respectively. The shape functions for each element are given by equation (2.29), where ξ and η are the natural coordinates of the element.

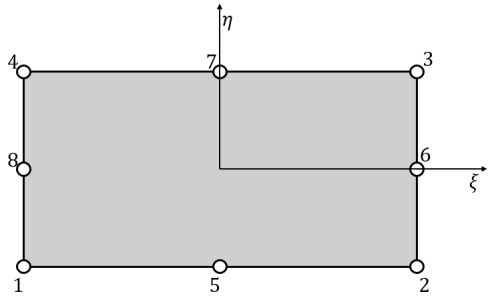

Figure 2.6: Eight-node serendipity quadratic element

$$\{N^e\} = \begin{Bmatrix} N_1^e \\ N_2^e \\ N_3^e \\ N_4^e \\ N_5^e \\ N_6^e \\ N_7^e \\ N_8^e \end{Bmatrix} = \begin{Bmatrix} \frac{1}{4}(1-\xi)(1-\eta)(-\xi-\eta-1) \\ \frac{1}{4}(1+\xi)(1-\eta)(\xi-\eta-1) \\ \frac{1}{4}(1+\xi)(1+\eta)(\xi+\eta-1) \\ \frac{1}{4}(1-\xi)(1+\eta)(-\xi+\eta-1) \\ \frac{1}{2}\left(1-\xi^2\right)(1-\eta) \\ \frac{1}{2}(1+\xi)\left(1-\eta^2\right) \\ \frac{1}{2}\left(1-\xi^2\right)(1+\eta) \\ \frac{1}{2}(1-\xi)\left(1-\eta^2\right) \end{Bmatrix} \tag{2.29}$$

The displacement vector of each element can be expressed as a function of the element nodal degrees of freedom:

$$\{d^e\} = \{N\}^T\{a^e\} = \sum_{i=1}^{8}\{N_i^e\}\{d_i^e\} = \begin{bmatrix} N_1^e & N_2^e & ... & N_8^e \end{bmatrix} \begin{Bmatrix} d_1^e \\ d_2^e \\ ... \\ d_8^e \end{Bmatrix} \tag{2.30}$$

where $\{d_i^e\}$ is the vector of nodal degrees of freedom of node i and is given, respectively, for FSDT and HSDT model, by:

$$\{d_i^e\}_{FSDT} = \begin{Bmatrix} u_{0i}^e & v_{0i}^e & w_{0i}^e & \theta_{xi}^e & \theta_{yi}^e \end{Bmatrix} \tag{2.31a}$$

$$\{d_i^e\}_{FSDT} = \begin{Bmatrix} u_{0i}^e & v_{0i}^e & w_{0i}^e & \theta_{xi}^e & \theta_{yi}^e & \theta_{zi}^e & u_{0i}^{*e} & v_{0i}^{*e} & w_{0i}^{*e} & \theta_{xi}^{*e} & \theta_{yi}^{*e} \end{Bmatrix} \tag{2.31b}$$

The equations of motion for the plate are obtained by applying the Hamilton's principle given by:

$$\delta \int_{t_1}^{t_2} L\, dt = 0 \tag{2.32}$$

where L is the Lagrangian of the system which can be calculated with the following equation:

$$L = T - \Pi \tag{2.33}$$

where T represents the kinetic energy and Π is the total potential energy of the plate. The kinetic energy is defined by:

$$T = \frac{1}{2}\int_V \rho\{\dot{u}\}^T\{\dot{u}\}\, dV \tag{2.34}$$

where ρ is the density and $\dot{u}$ represents the time derivative component of the displacement field vector, which can be written as:

$$\{u\} = [Z]\{d\} \tag{2.35}$$

where $[Z]$ depends on which model is being used, and is given by:

$$[Z]_{FSDT} = \begin{bmatrix} 1 & 0 & 0 & z & 0 \\ 0 & 1 & 0 & 0 & z \\ 0 & 0 & 1 & 0 & 0 \end{bmatrix} \tag{2.36a}$$

$$[Z]_{HSDT} = \begin{bmatrix} 1 & 0 & 0 & z & 0 & 0 & z^2 & 0 & 0 & z^3 & 0 \\ 0 & 1 & 0 & 0 & z & 0 & 0 & z^2 & 0 & 0 & z^3 \\ 0 & 0 & 1 & 0 & 0 & z & 0 & 0 & z^2 & 0 & 0 \end{bmatrix} \tag{2.36b}$$

$\{d\}$ is the vector of the mechanical degrees of freedom and is:

$$\{d\}_{FSDT} = \begin{Bmatrix} u_0 & v_0 & w_0 & \theta_x & \theta_y \end{Bmatrix}^T \tag{2.37a}$$

$$\{d\}_{HSDT} = \begin{Bmatrix} u_0 & v_0 & w_0 & \theta_x & \theta_y & \theta_z & u_0^* & v_0^* & w_0^* & \theta_x^* & \theta_y^* \end{Bmatrix}^T \tag{2.37b}$$

The potential energy Π is defined as:

$$\Pi = \sum_{i=1}^{NL} U_i - W \tag{2.38}$$

where U_i and W are the strain energy of each layer i and the work done by externally applied loads, respectively.

The strain energy of each layer is given by:

$$U_i = \frac{1}{2} \int_{V_i} \left(\{\sigma_i\}\{\varepsilon_i^L\} + \{\sigma_i^0\} 2 \{\varepsilon_i^{NL}\} \right) dV_i \tag{2.39}$$

where V_i represents the volume domain of the plate i. $\{\sigma_i\}$ and $\{\sigma_i^0\}$ are the stress and initial stress vectors, $\{\varepsilon_i^L\}$ and $\{\varepsilon_i^{NL}\}$ are the linear and non-linear strain vectors. For the element, equation (2.39) can be written as:

$$U_e = \frac{1}{2} \int_{A^e} \int_h \sigma_{ij} \varepsilon_{ij}^L \, dz \, dA^e + \frac{1}{2} \int_{A^e} \int_h \sigma_{ij}^0 2 \varepsilon_{ij}^{NL} \, dz \, dA^e \tag{2.40}$$

where A^e is the area of the element, h is the thickness of the layer and $i, j = x, y, z$.

The external work W can be calculated by:

$$W = \int_V \{d^T\}\{f_b\} \, dV + \int_S \{d^T\}\{f_s\} \, dS + \{d^T\}\{f_c\} \tag{2.41}$$

where $\{f_b\}$, $\{f_s\}$ and $\{f_c\}$ are, respectively, the vectors of body forces, surface tractions and concentrated forces. V and S represent volume and surface domains of the plate, respectively.

Mass Matrix

Integrating through the thickness the equation (2.34) can be written as:

$$\int_A \delta\{d\}^T [P] \{\ddot{d}\} \, dA \tag{2.42}$$

where A is the in-plane area of the plate and $[P]$ is obtained by:

$$[P] = \int_{-h/2}^{h/2} \rho [Z]^T [Z] \, dz \tag{2.43}$$

Combining equation (2.42) with equations (2.30) the mass matrix can be obtained by:

$$[M^e] = \int_A [N]^T \, [P] \, [N] \, dA \tag{2.44}$$

Changing coordinates from (x, y) to the natural coordinates (ξ, η) the element mass matrix is given by:

$$[M^e] = \int_{-1}^{+1} \int_{-1}^{+1} \left([N]^T [P] [N] \right) \det(J) \, d\xi \, d\eta \tag{2.45}$$

Linear Stiffness Matrix

Knowing the generalised displacement vector at all points within the element (d_i^e), the generalised linear strain vector at any point is given by:

$$\{\varepsilon^L\} = \sum_{i=1}^{8} [B_i] \{d_i^e\} \tag{2.46}$$

where the corresponding approximation of membrane, bending and shear can be written as:

$$\{\varepsilon^m\} = \sum_{i=1}^{8} [B_i^m] \{d_i^e\} \tag{2.47a}$$

$$\{\varepsilon^b\} = \sum_{i=1}^{8} [B_i^b] \{d_i^e\} \tag{2.47b}$$

$$\{\varepsilon^s\} = \sum_{i=1}^{8} [B_i^s] \{d_i^e\} \tag{2.47c}$$

Carrying on the integration in the thickness direction, and using equations (2.21) and (2.23) for the FSDT and equations (2.27) and (2.28) for the HSDT, the first term of equation (2.40) can be written as following:

$$\frac{1}{2} \int_{A^e} (\{\varepsilon_m\}^T [D_m] \{\varepsilon_m\} + \{\varepsilon_m\}^T [D_c] \{\varepsilon_b\} + \{\varepsilon_b\}^T [D_c] \{\varepsilon_m\} + \{\varepsilon_b\}^T [D_b] \{\varepsilon_b\} + \{\varepsilon_s\}^T [D_s] \{\varepsilon_s\}) \, dA^e \tag{2.48}$$

The internal linear strain energy expression in terms of the nodal displacements can be obtained substituting equation (2.46) into equation (2.48).

$$U_1^e = \frac{1}{2} \{a^e\}^T [K^e] \{a^e\} \tag{2.49}$$

Doing the same as before, and changing the coordinates from (x, y) to the natural coordinates (ξ, η)

the element stiffness matrix can be obtained by:

$$[K^e] = \int_{-1}^{+1}\int_{-1}^{+1} ([B_m]^T [D_m] [B_m] + [B_m]^T [D_c] [B_b] + [B_b]^T [D_c] [B_m] + [B_b]^T [D_c] [B_b] + [B_s]^T [D_s] [B_s]) \det(J)\, d\xi\, d\eta \quad (2.50)$$

Geometric Stiffness Matrix

Proceeding to the integration in the thickness direction, the second term of equation (2.40) can be expressed as:

$$\frac{1}{2}\int_{A^e} \{G'\}^T [\tau] \{G'\}\, dA^e \quad (2.51)$$

where $\{G'\}$ is an auxiliary vector given by:

$$\{G^{'}\} = \sum_{i=1}^{8} [G_i]\{d_i^e\} \quad (2.52)$$

$$\{G'\}_{FSDT} = \left\{\theta_x \quad \theta_y \quad \frac{\partial u_0}{\partial x} \quad \frac{\partial u_0}{\partial y} \quad \frac{\partial v_0}{\partial x} \quad \frac{\partial v_0}{\partial y} \quad \frac{\partial w_0}{\partial x} \quad \frac{\partial w_0}{\partial y} \quad \frac{\partial \theta_x}{\partial x} \quad \frac{\partial \theta_x}{\partial y} \quad \frac{\partial \theta_y}{\partial x} \quad \frac{\partial \theta_y}{\partial y}\right\}^T \quad (2.53a)$$

$$\{G'\}_{HSDT} = \{\theta_x \quad \theta_y \quad \theta_z \quad 2u_0^* \quad 2v_0^* \quad 2w_0^* \quad 3\theta_x^* \quad 3\theta_y^* \quad \frac{\partial u_0}{\partial x} \quad \frac{\partial u_0}{\partial y} \quad \frac{\partial v_0}{\partial x} \quad \frac{\partial v_0}{\partial y} \quad \frac{\partial w_0}{\partial x} \quad \frac{\partial w_0}{\partial y} \quad \frac{\partial \theta_x}{\partial x} \quad \frac{\partial \theta_x}{\partial y} \quad \frac{\partial \theta_y}{\partial x} \quad \frac{\partial \theta_y}{\partial y} \quad \frac{\partial \theta_z}{\partial x} \quad \frac{\partial \theta_z}{\partial y} \quad \frac{\partial u_0^*}{\partial x} \quad \frac{\partial u_0^*}{\partial y} \quad \frac{\partial v_0^*}{\partial x} \quad \frac{\partial v_0^*}{\partial y} \quad \frac{\partial w_0^*}{\partial x} \quad \frac{\partial w_0^*}{\partial y} \quad \frac{\partial \theta_x^*}{\partial x} \quad \frac{\partial \theta_x^*}{\partial y} \quad \frac{\partial \theta_y^*}{\partial x} \quad \frac{\partial \theta_y^*}{\partial y}\}^T \quad (2.53b)$$

The internal non-linear strain energy expression in terms of the nodal displacements can be obtained substituting equation (2.52) into equation (2.51), which presents the following form:

$$U_2^e = \frac{1}{2}\{a^e\}^T [K_G^e] \{a^e\} \quad (2.54)$$

Once again, changing the coordinates from (x, y) to the natural coordinates (ξ, η) the element geometric stiffness matrix is given by:

$$[K_G^e] = \int_{-1}^{+1}\int_{-1}^{+1} \left([G]^T [\tau] [G]\right) \det(J)\, d\xi\, d\eta \quad (2.55)$$

The initial stress state σ^0, required to formulate $[\tau]$, is computed with the displacement results obtained from a static analysis, using the constitutive relations and the displacement fields of each theory. The static analysis is done solving the following equation:

$$[K^e] \{a^e\} = \{F^e\} \quad (2.56)$$

where $\{F^e\}$ is the force vector given by:

$$\{F^e\} = \int_{-1}^{+1}\int_{-1}^{+1} \left(\{N\}^T\{f_b\}^e h + \{N\}^T\{f_s\}^e\right) \det(J)\; d\xi\, d\eta + \{N\}^T\{f_c\}^e \tag{2.57}$$

All the necessary integrations, to obtain the element matrices, are done numerically, using Gauss-Lagrange numerical integration, and selective integration is employed in order to avoid shear locking. For the membrane, bending, bending-membrane coupling terms of linear stiffness matrix, the geometric stiffness matrix, the force vector and the mass matrix was performed a 3×3 Gauss point integration. For the shear terms of the linear stiffness matrix and the post-stress computation a 2×2 Gauss point integration was used.

2.4 Vibration Analysis

It is possible to obtain an eigenvalue problem from equation 2.58, assuming periodic solutions in the form $\{u(x,y,t)\} = \{u(x,y)\}e^{i\omega t}$, being $\{u\}$ the displacement field vector.

$$[M]\{\ddot{u}\} + [K]\{u\} = 0 \tag{2.58}$$

Performing the eigenvalue problem shown on equation (2.59), on a structure, the free vibration frequencies can be obtained. Where ω is the free vibration frequency. The square root of the eigenvalues obtained are the free vibration frequencies for the different modes of vibration.

$$\left|[K] - \omega^2[M]\right| = 0 \tag{2.59}$$

The boundary conditions that the plates were under during this analysis were the same for all the models presented. All the structures studied were simply supported in all the four edges as shown in Figure 2.7. The details of the boundary conditions applied during this analysis can be seen on Table 2.1.

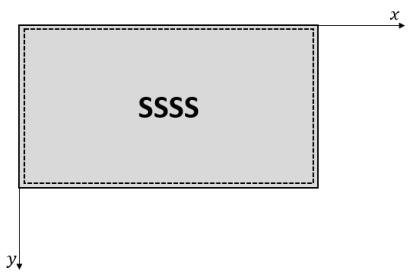

Figure 2.7: Boundary conditions

Table 2.1: Details of boundary conditions used for the vibration analysis for FSDT and HSDT

	FSDT
$x = 0, a$	$v_0 = w_0 = \theta_y = 0$
$y = 0, b$	$u_0 = w_0 = \theta_x = 0$
	HSDT
$x = 0, a$	$v_0 = w_0 = \theta_y = v_0^* = w_0^* = \theta_y^* = \theta_z = 0$
$y = 0, b$	$u_0 = w_0 = \theta_x = u_0^* = w_0^* = \theta_x^* = \theta_z = 0$

A vibration analysis was performed in an isotropic square plate with only a ply, with $a = b = 0.3$m, thickness of 0.003m and $\nu = 0.25$. The results obtained are shown in Table 2.2. It is important to mention that the results presented are non dimensional given by:

$$\bar{\omega} = \omega a^2 \sqrt{\frac{\rho h}{D}} \tag{2.60}$$

with

$$D = \frac{Eh^3}{12\left(1-\nu^2\right)} \tag{2.61}$$

The theoretical results presented were based on CLPT and calculated by [34]:

$$\omega = \sqrt{\frac{D}{\rho h}}\left[\left(\frac{m}{a}\right)^2 + \left(\frac{n}{b}\right)^2\right]\pi^2 \tag{2.62}$$

Table 2.2: Non dimensional free vibration frequency results for an isotropic square plate ($a/h = 100$)

Mode	$N \times N$	$\bar{\omega}$ FSDT	$\bar{\omega}$ HSDT	$\bar{\omega}$ Theoretical (CLPT)	Relative error (FSDT)	Relative error (HSDT)
(1,1)	2x2	33.1171	33.7461	19.739	67.775%	70.962%
	5x5	19.7615	19.7662	19.739	0.114%	0.138%
	10x10	19.7328	19.7329	19.739	0.031%	0.031%
	15x15	19.7325	19.7325	19.739	0.033%	0.033%
	20x20	19.7324	19.7324	19.739	0.033%	0.033%
(1,2)	2x2	310.6434	326.4562	49.348	529.495%	561.539%
	5x5	49.8831	49.9607	49.348	1.084%	1.242%
	10x10	49.3191	49.3194	49.348	0.0586%	0.058%
	15x15	49.3080	49.3080	49.348	0.081%	0.081%
	20x20	49.3063	49.3063	49.348	0.085%	0.085%
(2,1)	2x2	310.6434	327.2766	49.348	529.495%	563.201%
	5x5	49.8831	49.9607	49.348	1.084%	1.242%
	10x10	49.3191	49.3194	49.348	0.0586%	0.058%
	15x15	49.3080	49.3080	49.348	0.081%	0.081%
	20x20	49.3063	49.3063	49.348	0.085%	0.085%
(2,2)	2x2	306.7536	339.4727	78.957	288.507%	329.946%
	5x5	85.9242	87.1351	78.957	8.824%	10.358%
	10x10	78.8942	78.8989	78.957	0.079%	0.074%
	15x15	78.8534	78.8536	78.957	0.131%	0.131%
	20x20	78.8495	78.8495	78.957	0.136%	0.136%
(1,3)	2x2	668.9343	668.9343	98.696	577.772%	577.772%
	5x5	102.5280	102.9198	98.696	3.883%	4.280%
	10x10	98.6700	98.6715	98.696	0.026%	0.025%
	15x15	98.5540	98.5541	98.696	0.144%	0.144%
	20x20	98.5350	98.5350	98.696	0.163%	0.163%

Then an orthotropic square plate with only a ply, $a = b = 0.03$m and $a/h = 10$ was studied. The

results of the vibration analysis are presented in Table 2.3. The theoretical results used were found in [23] and were based on Reddy's HSDT. For this analysis the non dimensional free vibration frequencies are given by:

$$\bar{\omega} = \omega h \sqrt{\frac{\rho}{C_{11}}} \tag{2.63}$$

where C_{11} is the elastic constant with the value of 159.85GPa[23].

Table 2.3: Non dimensional free vibration frequency results for an orthotropic square plate ($a/h = 10$)

Mode	$N \times N$	$\bar{\omega}$ FSDT	$\bar{\omega}$ HSDT	$\bar{\omega}$ Theoretical (Reddy's HSDT)	Relative error (FSDT)	Relative error (HSDT)
(1,1)	2x2	0.0488	0.0490	0.0474	2.954%	3,376%
	5x5	0.0474	0.0474	0.0474	0%	0%
	10x10	0.0474	0.0474	0.0474	0%	0%
	15x15	0.0474	0.0474	0.0474	0%	0%
	20x20	0.0474	0.0474	0.0474	0%	0%
(1,2)	2x2	0.1224	0.1250	0.1033	18.490%	21.007%
	5x5	0.1035	0.1035	0.1033	0.194%	0.194%
	10x10	0.1032	0.1032	0.1033	0.097%	0.097%
	15x15	0.1032	0.1032	0.1033	0.097%	0.097%
	20x20	0.1032	0.1032	0.1033	0.097%	0.097%
(2,1)	2x2	0.1453	0.1491	0.1188	22.306%	25.505%
	5x5	0.1191	0.1192	0.1188	0.253%	0.337%
	10x10	0.1187	0.1188	0.1188	0.084%	0%
	15x15	0.1187	0.1188	0.1188	0.084%	0%
	20x20	0.1187	0.1188	0.1188	0.084%	0%
(2,2)	2x2	0.3018	0.2190	0.1694	78.158%	29.280%
	5x5	0.1699	0.1700	0.1694	0.295%	0.354%
	10x10	0.1692	0.1693	0.1694	0.118%	0.059%
	15x15	0.1692	0.1692	0.1694	0.118%	0.118%
	20x20	0.1692	0.1692	0.1694	0.118%	0.118%
(1,3)	2x2	0.3276	0.3027	0.1888	73.517%	60.328%
	5x5	0.1915	0.1916	0.1888	1.430%	1.483%
	10x10	0.1886	0.1886	0.1888	0.106%	0.106%
	15x15	0.1884	0.1885	0.1888	0.212%	0.159%
	20x20	0.1884	0.1884	0.1888	0.212%	0.212%

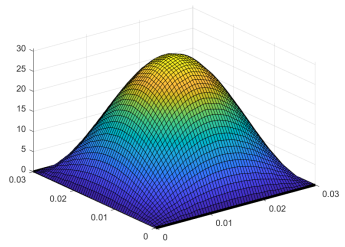

(a) Mode (1,1)

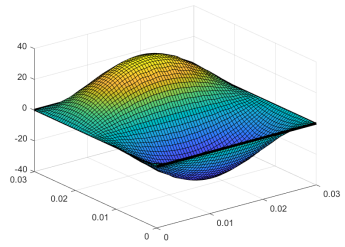

(b) Mode (1,2)

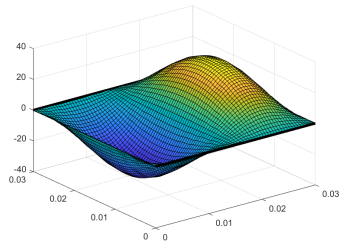

(c) Mode (2,1)

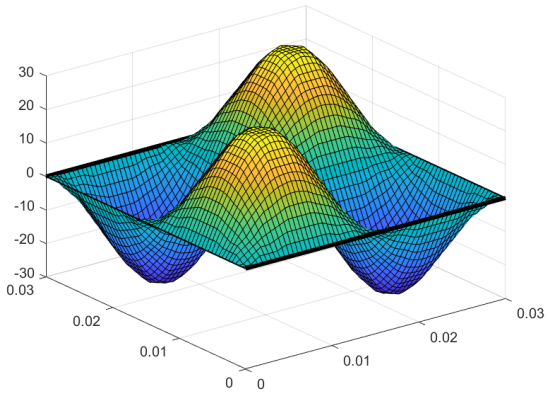

(d) Mode (2,2)

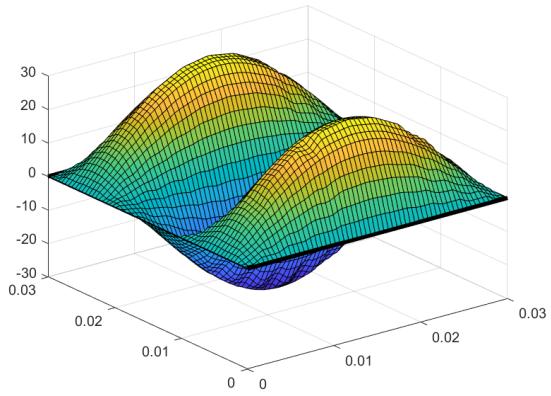

(e) Mode (1,3)

Figure 2.8: Vibration Modes

The results presented on Tables 2.2 and 2.3 allow to study, not only, the convergence but also the accuracy of the results obtained.

Table 2.2 shows that the results obtained, for both FSDT and HSDT, converge after a mesh size of 10×10 for all the modes studied for the isotropic plate. Since the orthotropic plate is a thick plate, where convergence is faster achieved, and the theoretical theory used is more suitable the results exhibited on Table 2.3 show a perfect convergence achieved. For both models, this convergence is accomplished after a mesh size of 5×5 for mode (1,1) and after a mesh size of 10×10 for all the other modes.

For the isotropic plate, after convergence is accomplished, the relative error of the free vibration frequencies, for both FSDT and HSDT models, are lower than 1% for all modes studied. Analysing the results obtained for the orthotropic plate, it is possible to say that, after convergence is achieved, the relative error of the free vibration frequencies of the first three modes is lower than 0.1%, for both FSDT and HSDT models. For the modes (2,2) and (1,3) the relative error is lower than 0.2%, for both models, for a mesh size of 10×10.

From this analysis it is possible to validate the formulations done for the mass matrix and linear stiffness matrix, for both FSDT and HSDT models. As mention in section 1.3, in this work, the formulations of the matrices K and K_G are the ones done in [32] where they were already validated. Then, it is possible now to use with confidence the models and formulations presented in this section to build more models and/or make other analysis with them.

Chapter 3

Dynamic Instability Analysis

In this chapter the numerical model to analyse the dynamic instability of structures is presented.

After joining this model with the theories and formulations presented in chapter 2 results for, both the FSDT model and HSDT model, are presented.

3.1 Dynamic Instability

There is different physical explanations for the phenomenon of instability. An easy definition that can be intuitively explained by the illustrative figures shown bellow is the energy method. This definition has per base the Lagrange-Dirichlet theorem and states that the equilibrium of a conservative system will be stable if and only if the total potential energy — the sum of the potential energies associated with deformation and strain — takes a strict local minimum. In Figure 3.1 the ball represents the system which is initially in equilibrium. Figure 3.1(a) represents a stable state of a system since a perturbation will move the ball from its equilibrium position but it will roll back to its equilibrium position (position of minimal potential energy). On the other side, in Figure 3.1(b) after a perturbation the ball will move further away from its equilibrium position. Finally, Figure 3.1(c) depicts a neutral state since if the system suffers a perturbation it will move in the plane assuming a new equilibrium state without any difference in the energy state.

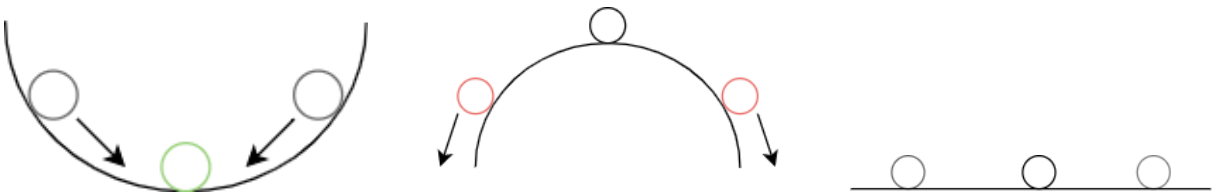

(a) Stable (b) Unstable (c) Neutral

Figure 3.1: Instability phenomenon

Another definition that is also widely used is based on the classical stability definition by Lyapunov, which states that the fact that all solutions to the evolution equations governing the problem, starting

from adjacent initial conditions, remain consistently close to this state is a necessary and sufficient requirement for the stability of an equilibrium point.

In contrast to their static counterparts, dynamic instability events occur at a non-zero critical frequency and entail all mechanical issues where the inclusion of time cannot be avoided. The most common case of dynamic instability is when dynamic loads, including periodic loads, are applied to mechanical structures.

3.2 Numerical Model

To find the regions of dynamic instability of a structure it is useful to use the theory of systems of Mathieu-Hill differential equations with periodic coefficients. It is, for this reason, important to analyse the conditions that the structure being studied is subjected to in order to be possible to include the equations of motion in the class of Mathieu-Hill differential equations with periodic coefficients.

The structural systems that are being studied in this work the equations of motion that are Mathieu-Hill equations can be presented in the following form:

$$[M]\{\ddot{x}\} + [K]\{x\} - P(t)[K_G]\{x\} = 0 \tag{3.1a}$$

$$[K]^{-1}[M]\{\ddot{x}\} + [I]\{x\} - P(t)[K]^{-1}[K_G]\{x\} = 0 \tag{3.1b}$$

$$[K]^{-1}[M]\{\ddot{x}\} + \left[[I] - P_S[K]^{-1}[K_G] - P_d[K]^{-1}[K_G]\cos\theta t\right]\{x\} = 0 \tag{3.1c}$$

where $[M]$, $[K]$ and $[K_G]$ are, respectively, the mass matrix, the stiffness matrix and the geometric stiffness matrix. $P(t)$ is the periodic force that can be presented as $P(t) = P_S + P_d\cos(\theta t)$. P_S is the static component and P_d is the dynamic component of the applied load. When P_d is different than zero the load P will vary with time and the system can not be considered as static.

The method suggested by Bolotin [13] was used to determine the regions of dynamic instability. The boundaries between the dynamic stability and instability regions are separated by periodic solutions with period T and 2T in equation (3.1c), being $T = \frac{2\pi}{\theta}$. These solutions can be expanded into Fourier series. Periodic solutions with period 2T and T in equation (3.1c) present, respectively, the following form:

$$x(t) = \sum_{k=1,3,5}^{\infty} a_k \sin\frac{k\theta t}{2} + b_k \cos\frac{k\theta t}{2} \qquad \text{(period } 2T\text{)} \tag{3.2}$$

$$x(t) = b_0 + \sum_{k=2,4,6}^{\infty} a_k \sin\frac{k\theta t}{2} + b_k \cos\frac{k\theta t}{2} \qquad \text{(period } T\text{)} \tag{3.3}$$

To be precise, two solutions of identical periods bound the region of dynamic instability and two solutions of different periods bound the region of dynamic stability. Substituting (3.2) or (3.3) in equation (3.1c) and equating the coefficients of identical $\sin\frac{k\theta t}{2}$ and $\cos\frac{k\theta t}{2}$ a system of linear homogeneous algebraic equations are obtained with infinite equations and infinite unknowns a_k and b_k. The system of linear homogeneous equations has non-zero solutions only if the determinant of the coefficients of the

system is equal to zero. The equations of critical frequencies are then obtained from the condition that equation (3.1c) presents periodic solutions if the obtained determinants of the homogeneous systems are zero.

The equation of boundary frequencies that allows to find the regions of instability which are bounded by periodic solutions with a period 2T is:

$$\begin{vmatrix} [I] - (P_S \pm \frac{P_d}{2})[K]^{-1}[K_G] - \frac{\theta^2}{4}[K]^{-1}[M] & -\frac{P_d}{2}[K]^{-1}[K_G] & 0 & ... \\ -\frac{P_d}{2}[K]^{-1}[K_G] & [I] - P_S[K]^{-1}[K_G] - \frac{9\theta^2}{4}[K]^{-1}[M] & -\frac{P_d}{2}[K]^{-1}[K_G] & ... \\ 0 & -\frac{P_d}{2}[K]^{-1}[K_G] & [I] - P_S[K]^{-1}[K_G] - \frac{25\theta^2}{4}[K]^{-1}[M] & ... \\ ... & ... & ... & ... \end{vmatrix} = 0 \quad (3.4)$$

For the regions of instability bounded by the periodic solutions with a period T, the equations of boundary frequencies are:

$$\begin{vmatrix} [I] - P_S[K]^{-1}[K_G] - \theta^2[K]^{-1}[M] & -\frac{P_d}{2}[K]^{-1}[K_G] & 0 & ... \\ -\frac{P_d}{2}[K]^{-1}[K_G] & [I] - P_S[K]^{-1}[K_G] - 4\theta^2[K]^{-1}[M] & -\frac{P_d}{2}[K]^{-1}[K_G] & ... \\ 0 & -\frac{P_d}{2}[K]^{-1}[K_G] & [I] - P_S[K]^{-1}[K_G] - 9\theta^2[K]^{-1}[M] & ... \\ ... & ... & ... & ... \end{vmatrix} = 0 \quad (3.5a)$$

$$\begin{vmatrix} [I] - P_S[K]^{-1}[K_G] & -\frac{P_d}{2}[K]^{-1}[K_G] & 0 & 0 & ... \\ -P_d[K]^{-1}[K_G] & [I] - P_S[K]^{-1}[K_G] - \theta^2[K]^{-1}[M] & -\frac{P_d}{2}[K]^{-1}[K_G] & 0 & ... \\ 0 & -\frac{P_d}{2}[K]^{-1}[K_G] & [I] - P_S[K]^{-1}[K_G] - 4\theta^2[K]^{-1}[M] & -\frac{P_d}{2}[K]^{-1}[K_G] & ... \\ 0 & 0 & -\frac{P_d}{2}[K]^{-1}[K_G] & [I] - P_S[K]^{-1}[K_G] - 9\theta^2[K]^{-1}[M] & ... \\ ... & ... & ... & ... & ... \end{vmatrix} = 0 \quad (3.5b)$$

where θ is the frequency of the external load and [I] is the identity matrix.

From these equations, the equations to calculate the different regions of dynamic instability for the different approximations are obtained.

The boundaries for the principal/first region of instability with first order approximation are obtained by solving equation (3.6) (i.e. determinant of first-order equal to zero), leading to θ_1. The second order approximation for the boundaries for the same region is given by equation (3.7) (i.e. determinant of second-order equal to zero), leading to θ_2.

$$[I] - (P_S \pm \frac{P_d}{2})[K]^{-1}[K_G] - \frac{\theta^2}{4}[K]^{-1}[M] = 0 \quad (3.6)$$

$$\begin{vmatrix} [I] - (P_S \pm \frac{P_d}{2})[K]^{-1}[K_G] & -\frac{P_d}{2}[K]^{-1}[K_G] \\ -\frac{P_d}{2}[K]^{-1}[K_G] & [I] - P_S[K]^{-1}[K_G] - \frac{9\theta_1^2}{4}[K]^{-1}[M] \end{vmatrix} - \theta_2^2 \begin{vmatrix} \frac{1}{4}[K]^{-1}[M] & 0 \\ 0 & 0 \end{vmatrix} = 0 \quad (3.7)$$

The first-order approximation for both boundaries (left and right) for the second region of instability, leading to θ_1, are given by:

$$\left| [I] - P_S[K]^{-1}[K_G] - \theta^2[K]^{-1}[M] = 0 \right| \quad (3.8)$$

The second approximation for the second region of instability can be obtained from:

$$\begin{vmatrix} [I] - P_S[K]^{-1}[K_G] & -\frac{P_d}{2}[K]^{-1}[K_G] \\ -P_d[K]^{-1}[K_G] & [I] - P_S[K]^{-1}[K_G] \end{vmatrix} - \theta^2 \begin{vmatrix} 0 & 0 \\ 0 & [K]^{-1}[M] \end{vmatrix} = 0 \tag{3.9a}$$

$$\begin{vmatrix} [I] - P_S[K]^{-1}[K_G] & -\frac{P_d}{2}[K]^{-1}[K_G] \\ -\frac{P_d}{2}[K]^{-1}[K_G] & [I] - P_S[K]^{-1}[K_G] - 4\theta_1^2[K]^{-1}[M] \end{vmatrix} - \theta_2^2 \begin{vmatrix} [K]^{-1}[M] & 0 \\ 0 & 0 \end{vmatrix} = 0 \tag{3.9b}$$

It is easy to realise that these equations can be solved as eigenvalue problems.

3.3 Validation Case - Beam

First, the dynamic instability numerical model was applied to a beam, which is a simpler structure to analyse. This exercise will be helpful to validate the model and if the results are good it will allow to apply the model with confidence to more complex structures such as, isotropic, orthotropic, laminated composite and sandwich plates.

The dynamic stability analysis is performed to a HEB 200 beam, represented in Figure 3.2, with a length of 7m, $E = 2.1 \times 10^{11}$N/m^2, $J = 2003 \times 10^{-8}$m^4 and $m = 61.3$Kg/m, being $P(t) = P_s + P_d \cos \theta t$ with $P_s = 0$. Due to its boundary condition the constrained degrees of freedoms are 1 and 9. It is employed a finite element discretization with four Euler-Bernoulli beam elements without axial deformability.

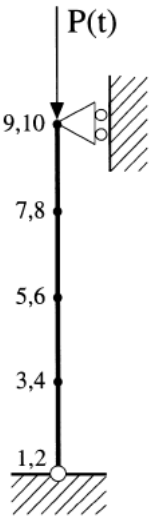

Figure 3.2: Beam discretization [12]

Figure 3.3 depicts the first and second approximations for the first and second instability dynamic regions of the beam under study.

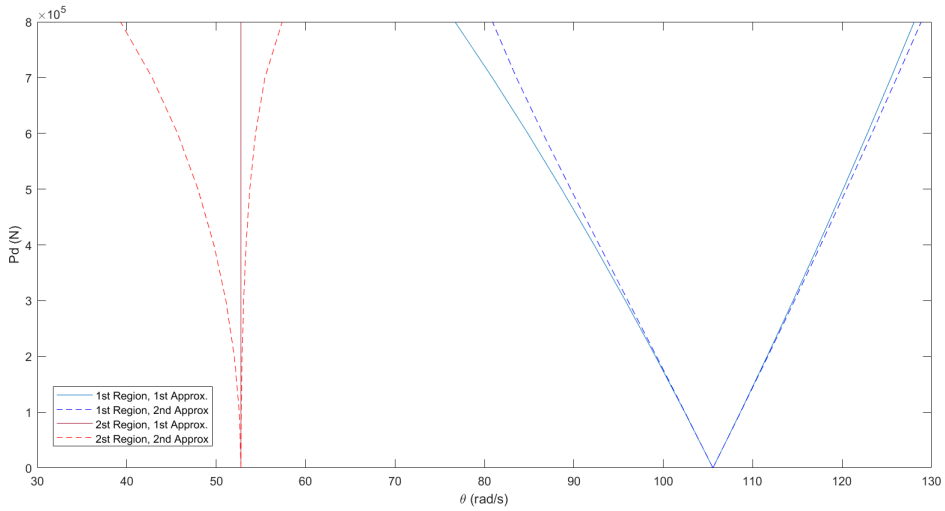

Figure 3.3: First and second approximation of the first and second dynamic instability region for the beam

Table 3.1 presents the values of the excitation frequencies, for the corresponding dynamic load (P_d), of the boundaries of the dynamic instability regions. θ_1 are the values of the left boundary and θ_2 the ones of the right boundary. The table also shows the values presented in Briseghella et al. [12]. It is relevant to mention that these values from literature were obtained from the graphs presented in [12] which can involve some error and uncertainty in the values.

Table 3.1: Frequency (Hz) of the boundary of the instability regions for a beam

P_d(N)	Present						Briseghella et al.[12]					
	Principal Region				Second Region		Principal Region				Second Region	
	1^{st} Approx.		2^{nd} Approx		2^{nd} Approx.		1^{st} Approx.		2^{nd} Approx		2^{nd} Approx.	
	θ_1	θ_2	θ_1	θ_2	θ_1	θ_2	θ_1	θ_2	θ_1	θ_2	θ_1	θ_2
0	105.6	105.6	105.6	105.6	52.78	52.78	105.66	105.66	105.66	105.66	52.61	52.61
400000	92.26	117.3	92.83	117.6	49.75	53.35	92.26	117.47	92.98	117.77	49.53	52.83
800000	76.71	128.1	80.9	128.8	39.3	57.4	76.67	128.11	80.87	128.88	39.18	53.71

To better compare the results obtained with the ones present in the literature, Table 3.2 indicates the relative deviations between both results.

Table 3.2: Relative deviations of frequency θ_1 and θ_2 (%)

P_d(N)	Principal Region				Second Region	
	1^{st} Approx.		2^{nd} Approx.		2^{nd} Approx.	
	θ_1	θ_2	θ_1	θ_2	θ_1	θ_2
0	0.06%	0.06%	0.06%	0.06%	0.32%	0.32%
400000	0%	0.14%	0.16%	0.14%	0.44%	0.98%
800000	0.05%	0.01%	0.04%	0.06%	0.31%	6.87%

From Tables 3.1 and 3.2 it is possible to conclude that the results obtained in this work were in accordance with the ones found in the literature. In fact, the majority of them are lower than 0.5% which shows a great accuracy on the results obtained. Therefore this analysis validates the model proposed to study the dynamic instability of structures.

3.4 Results

After presenting all the models and formulations, that were used in this work to study the dynamic instability of isotropic, orthotropic, composite laminated and sandwich plates, it is, now, possible to present the results obtained for the different plates under analysis. In section 2.4, it was shown that the convergence is already accomplished for a mesh of 10x10. Therefore, that will be the mesh size used in this section to compute the results for the dynamic instability analysis. Figure 3.4 depicts the boundary conditions and the location of the uniaxial load applied to all the plates studied.

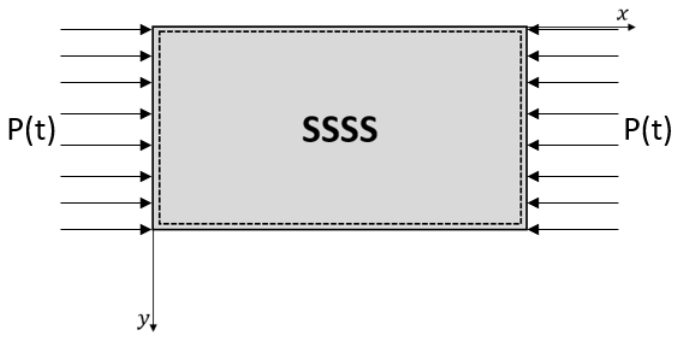

Figure 3.4: Plate Geometry

3.4.1 Isotropic Plate

The analysis of the dynamic instability of an isotropic square plate with Young's modulus of 70GPa, $\rho = 1543$Kg/m, $\nu = 0.25$, thickness of 3mm and a ratio $a/h = 100$ was performed.

In Figure 3.5 the results for the first region of instability are presented as a plot of frequency (θ) against β, that is the dynamic load factor used to obtained P_d as a function of the buckling load ($P_d = \beta N_{cr}$). The area in light blue, in Figure 3.5(b), is the instability region, so points in that area lead to a behaviour of dynamic instability of the structure under study. The area outside is the stable region, which means that any point in that area presents a stable behaviour.

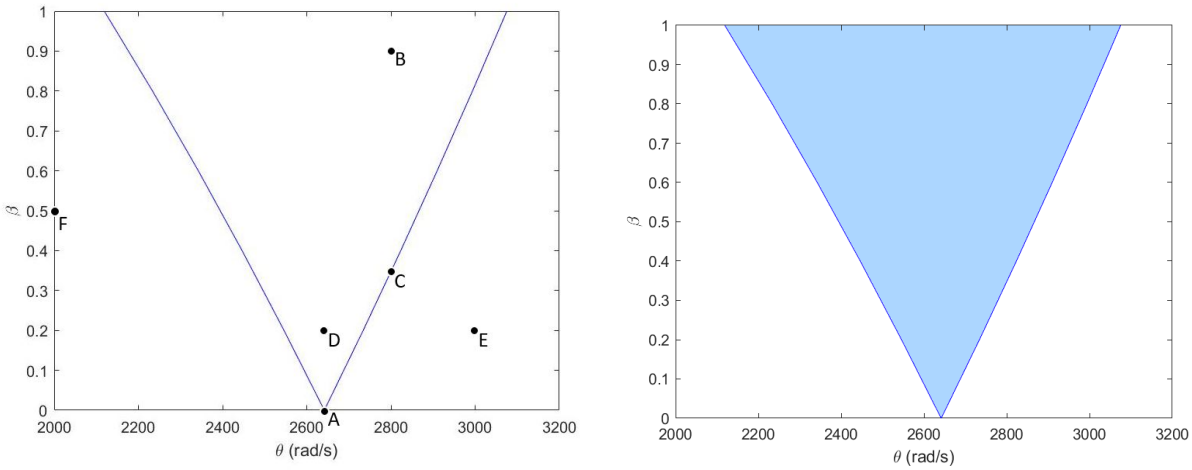

(a) Pointing out different instability regions

(b) Principal Region

Figure 3.5: Dynamic instability region for an isotropic plate

Adding equation (3.7) to the computational process the second approximation for the principal region of dynamic instability is obtained. Evolving the analysis, and, also, adding equations (3.8) and (3.9), the first and second approximation for the second region of instability are obtained. Both approximations for the first and second region are shown in Figure 3.6.

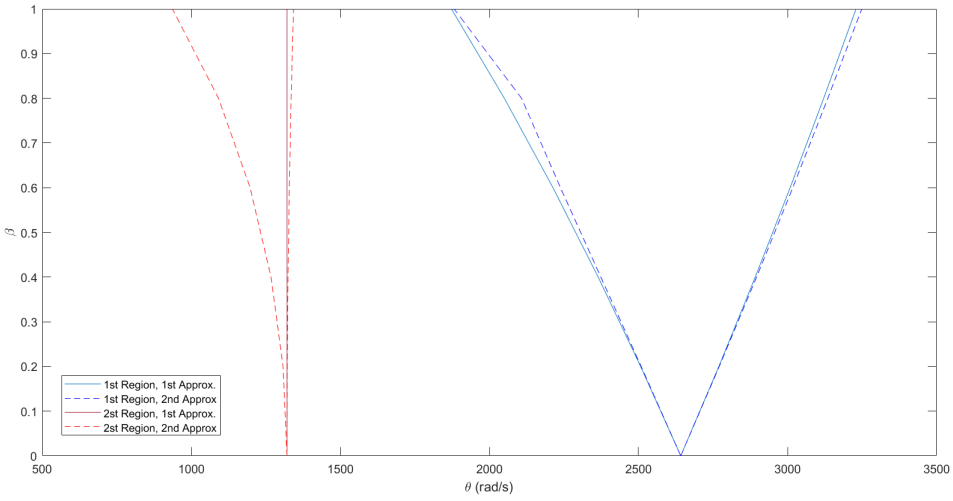

Figure 3.6: First and second approximation of the first and second dynamic instability region for an isotropic plate

To better understand the dynamic instability region and to verify the reliability of those regions, a direct integration using Newmark's Method was performed. The time increment used is $\Delta t = 9 \times 10^{-5}$s. An initial displacement of 0.0012m was imposed to the w_0 degree of freedom on the central node of the plate. The load cases studied are presented in Table 3.3 and their location on the dynamic instability region can be seen in Figure 3.5(a). The results for the different points are depicted in Figures 3.7(a-f).

Table 3.3: Load cases used to obtain the displacement vs time diagrams

	θ (rad/s)	P_d (N)	β
A	2642	0	0
B	2800	93000	0.91
C	2831	30820.2	0.3
D	2642	21000	0.2
E	3000	21000	0.2
F	2000	51000	0.5

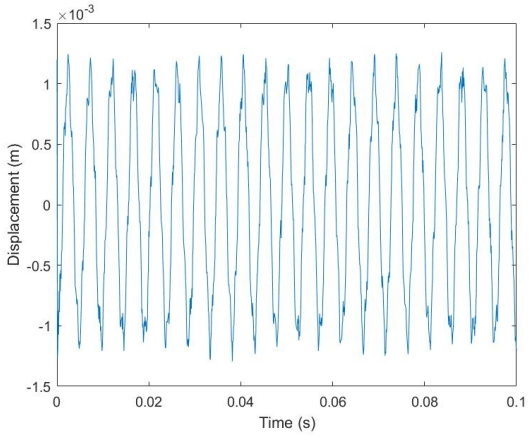

(a) Point A

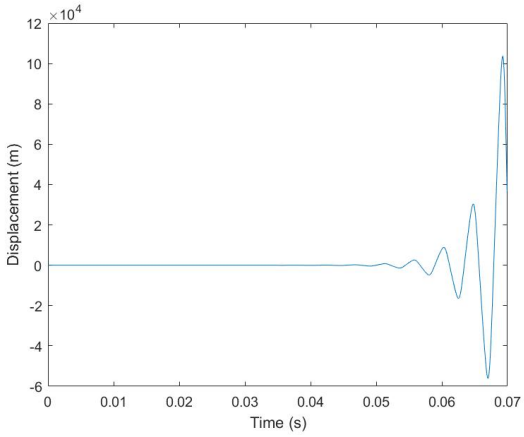

(b) Point B

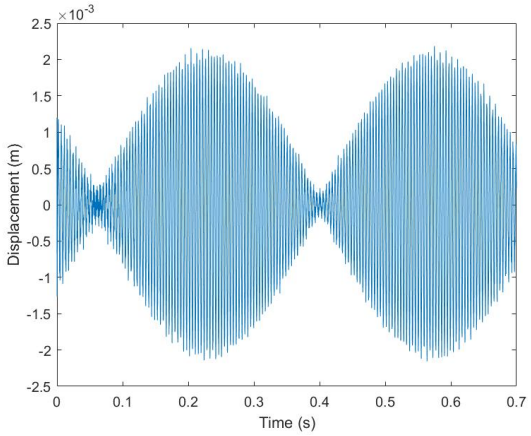

(c) Point C

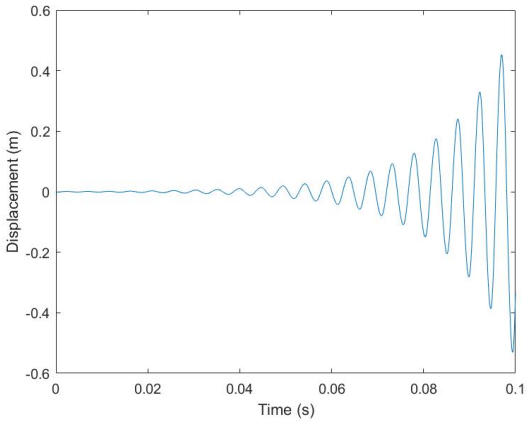

(d) Point D

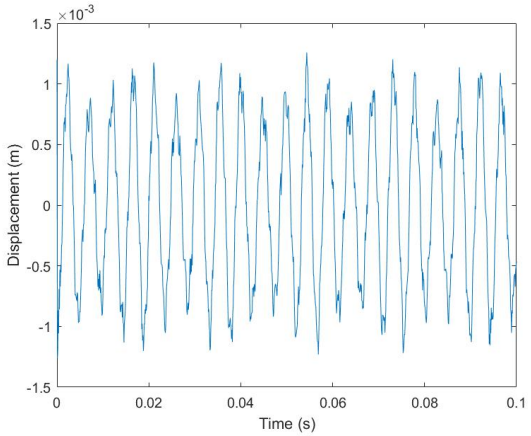

(e) Point E

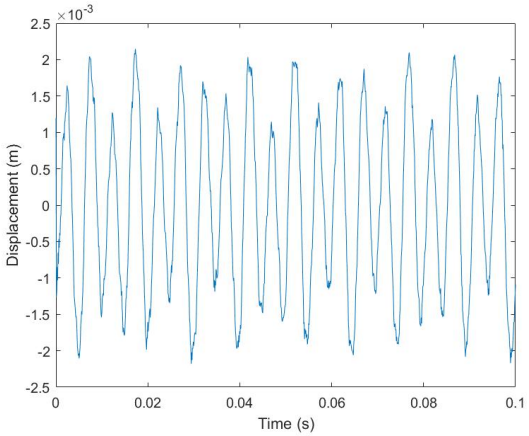

(f) Point F

Figure 3.7: Displacement vs Time diagrams

Studying the same plate as before, but computing the principal dynamic instability region as a plot of frequency ratio (θ/ω), ω being the natural frequency, against β, the results obtained can be seen in Figure 3.8(a) for the FSDT model and Figure 3.8(b) for the HSDT model.

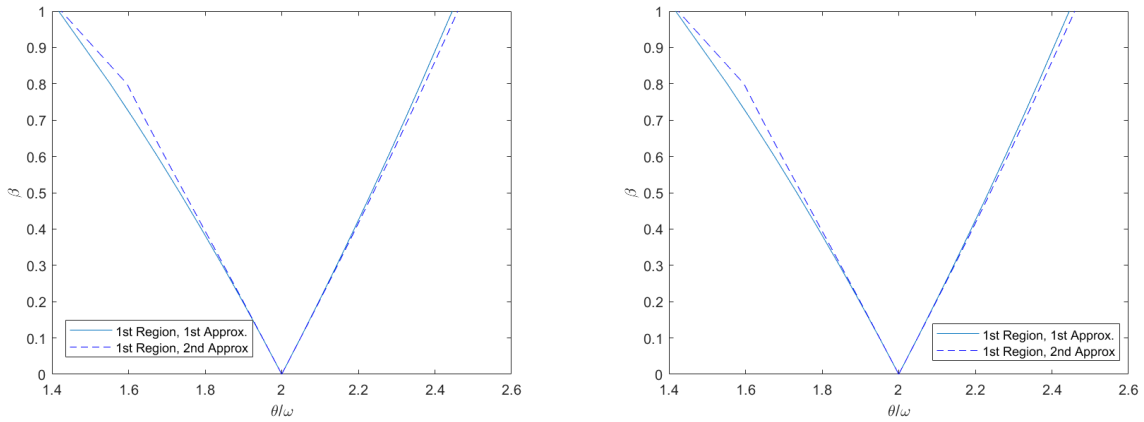

(a) using FSDT model

(b) using HSDT model

Figure 3.8: First and second approximation to principal region of dynamic instability for a square isotropic plate

Tables 3.4 and 3.5 present the values of frequency ratio ($\Omega = \theta/\omega$) in the first region of dynamic instability boundaries, with varying β, for the FSDT and HSDT model, respectively. Ω_1 are the values of the left boundary and Ω_2 the ones of the right boundary. These tables, also, present the results from Ramana Reddy et al. [21]. Table 3.6 shows the relative deviations between the results obtained in this work and the ones from [21].

Table 3.4: Variation of frequency ratios Ω_1 and Ω_2 for the first region of dynamic instability using FSDT model

β	1^{st} Approx.		2^{nd} Approx.		Ramana Reddy et al.[21]	
	Ω_1	Ω_2	Ω_1	Ω_2	Ω_1	Ω_2
0	2.000	2.000	2.000	2.000	2.0000	2.0000
0.1	1.950	2.049	1.950	2.049	1.9493	2.0493
0.2	1.898	2.097	1.900	2.098	1.8973	2.0976
0.3	1.845	2.144	1.848	2.146	1.8473	2.1447
0.4	1.790	2.189	1.797	2.193	1.7888	2.1908
0.5	1.734	2.234	1.746	2.239	1.7320	2.2360
0.6	1.676	2.278	1.694	2.285	1.6733	2.2803
0.7	1.615	2.321	1.644	2.329	1.6124	2.3237
0.8	1.552	2.363	1.596	2.374	1.5491	2.3664
1	1.418	2.445	1.424	2.460	1.4142	2.4493

Table 3.5: Variation of frequency ratios Ω_1 and Ω_2 for the first region of dynamic instability using HSDT model

β	1^{st} Approx.		2^{nd} Approx.		Ramana Reddy et al.[21]	
	Ω_1	Ω_2	Ω_1	Ω_2	Ω_1	Ω_2
0	2.000	2.000	2.000	2.000	2.0000	2.0000
0.1	1.950	2.049	1.950	2.049	1.9493	2.0493
0.2	1.898	2.097	1.900	2.098	1.8973	2.0976
0.3	1.845	2.144	1.848	2.146	1.8473	2.1447
0.4	1.790	2.189	1.797	2.193	1.7888	2.1908
0.5	1.734	2.234	1.746	2.239	1.7320	2.2360
0.6	1.676	2.278	1.695	2.285	1.6733	2.2803
0.7	1.615	2.321	1.644	2.329	1.6124	2.3237
0.8	1.552	2.363	1.596	2.374	1.5491	2.3664
1	1.418	2.445	1.424	2.460	1.4142	2.4493

Table 3.6: Relative deviations of frequency ratios Ω_1 and Ω_2 $(\%)$

β	FSDT				HSDT			
	1^{st} Approx.		2^{nd} Approx.		1^{st} Approx.		2^{nd} Approx.	
	Ω_1	Ω_2	Ω_1	Ω_2	Ω_1	Ω_2	Ω_1	Ω_2
0	0%	0%	0%	0%	0%	0%	0%	0%
0.1	0.04%	0.01%	0.04%	0.01%	0.04%	0.01%	0.04%	0.01%
0.2	0.04%	0.03%	0.14%	0.02%	0.04%	0.03%	0.14%	0.02%
0.3	0.12%	0.03%	0.04%	0.06%	0.12%	0.03%	0.04%	0.06%
0.4	0.07%	0.08%	0.46%	0.10%	0.07%	0.08%	0.46%	0.10%
0.5	0.12%	0.09%	0.81%	0.13%	0.12%	0.09%	0.81%	0.13%
0.6	0.16%	0.10%	1.30%	0.21%	0.16%	0.10%	1.24%	0.21%
0.7	0.16%	0.12%	1.96%	0.23%	0.16%	0.12%	1.96%	0.23%
0.8	0.19%	0.14%	3.03%	0.32%	0.19%	0.14%	3.03%	0.32%
1	0.27%	0.18%	0.69%	0.44%	0.27%	0.18%	0.69%	0.44%

Conclusions

Figures 3.7, besides allowing to understand better how the dynamic instability region is translated in the plate behaviour, it also shows that the boundaries obtained are quite good. Points F and E that are in the stable area present, in Figures 3.7(e) and (f), respectively, a stable behaviour since the amplitude of the displacement is the same through time. On the other hand, Figures 3.7(b) and (d) show that the points B and D are, clearly unstable. Both diagrams present an increasing of the amplitude of the

displacement with time, which is an unstable behaviour. Finally, Points A and C that are both in the boundary between the stable and unstable region present different behaviours. Figure 3.7(a) shows that the amplitude of motion is constant. Although, Figure 3.7(c) depicts a beat-frequency oscillation. This phenomenon happens when the plate vibrates with two different frequencies that interfere with each other. The oscillation amplitudes add or subtract themselves as a result of this discrepancy in vibrational frequencies due to a time variable phase difference between the components of the motion, and the resulting oscillation amplitude takes values between the sum and the difference between the corresponding amplitudes.

Moreover, the results just presented allow to conclude that the model used is valid in its generality. From Figures 3.8 and Table 3.6 it becomes clear that the results obtained are in accordance with the ones found in the literature. Actually, the relative deviations are lower than 2% for both approximations and both models. In general, the second approximation presents higher deviations than the first approximation. This can be explained by the fact that in the literature only results for the first approximation were found and the results obtained in this work for the second approximation are compared with the ones from the first. Even though it was not presented in the graphics obtained, the point of the left boundary of the second approximation for $\beta = 0.9$ shows an unexpected jump, for both the FSDT and HSDT, due to numerical problems that occur in that area.

It is relevant to mention that both models FSDT and HSDT presented really similar results. From tables 3.4 and 3.5 it is clear that the majority of the results are the same for both models, and the ones that differ, the difference is almost irrelevant.

3.4.2 Orthotropic Plate

In the study of the dynamic instability of an orthotropic plate the ply studied was a square plate with $a/h = 100$ and $a = b = 1$m. The material properties are $E_1 = 173$GPa, $E_2 = 33.1$GPa, $G_{12} = 9.38$GPa, $\nu = 0.25$ and density of 1000kg/m^3.

The results obtained for the principal region of dynamic instability, as a plot of frequency θ against the dynamic load factor β, are presented in Figure 3.9(a) and 3.9(b) for the FSDT and HSDT model, respectively.

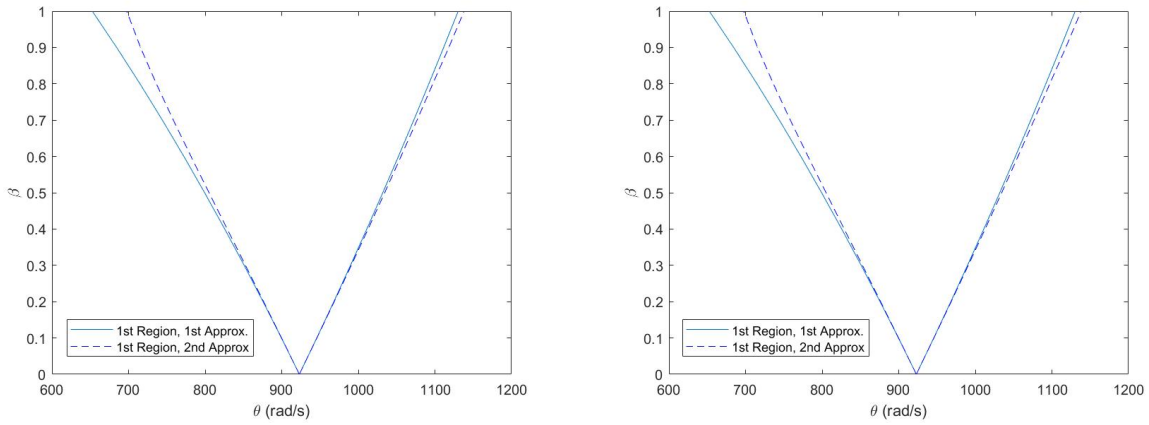

(a) using FSDT model

(b) using HSDT model

Figure 3.9: First and second approximation to principal region of dynamic instability for a square orthotropic plate

The resonance frequencies of the boundary of the instability region obtained for both models, and for both approximations, are presented in Table 3.7. That table also shows the results obtained for the same plate in the work developed by Loja et al.[17].

Table 3.7: Frequency (rad/s) of the boundary of the first region of instability for an orthotropic square plate

	FSDT				HSDT				Loja et al.[17]			
β	1^{st} Approx.		2^{nd} Approx.		1^{st} Approx.		2^{nd} Approx.		1^{st} Approx.		2^{nd} Approx.	
	θ_1	θ_2	θ_1	θ_2	θ_1	θ_2	θ_1	θ_2	θ_1	θ_2	θ_1	θ_2
0	923.0	923.0	923	923	923	923	923	923	921.48	921.48	921.48	921.48
0.5	799.3	1032	805.1	1034	799.3	1032	805.1	1034	802.05	1025.64	806.30	1027.29
1	652.7	1130	697.7	1138	625.7	1130	697.7	1138	658.63	1119.01	694.47	1123.74

To make it easier to compare the results presented, Table 3.8 shows the deviation of the results obtained for each model, FSDT and HSDT, and the ones presented in [17]. Since Loja et al. [17] presented results for both approximations, each approximation was compared with the respective approximation.

Table 3.8: Relative deviations of frequency θ_1 and θ_2 (%)

	FSDT				HSDT			
β	1^{st} Approx.		2^{nd} Approx.		1^{st} Approx.		2^{nd} Approx.	
	θ_1	θ_2	θ_1	θ_2	θ_1	θ_2	θ_1	θ_2
0	0.16%	0.16%	0.16%	0.16%	0.16%	0.16%	0.16%	0.16%
0.5	0.34%	0.62%	0.15%	0.65%	0.34%	0.62%	0.15%	0.65%
1	0.90%	0.98%	0.47%	1.27%	0.90%	0.98%	0.47%	1.27%

Figure 3.10 depicts the first and second approximation for both, the principal and second instability

regions, for the plate studied in this section. The model used to obtained this figure was FSDT due to the easier computational effort needed without losing accuracy of the results obtained as already shown previously.

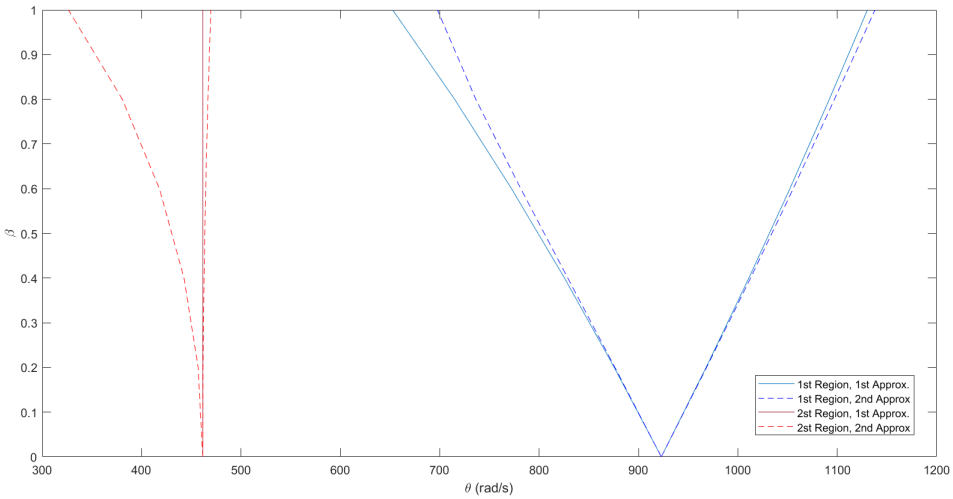

Figure 3.10: First and second approximation of the first and second dynamic instability region for an orthotropic plate

The dimensions of the plate will affect deeply the location of the dynamic instability region. One important factor that will have an impact is the thickness of the plate. In order to analyse its impact a dynamic instability analysis was performed for the orthotropic plate already studied with different ratios b/h. The results obtained are presented in Figure 3.11.

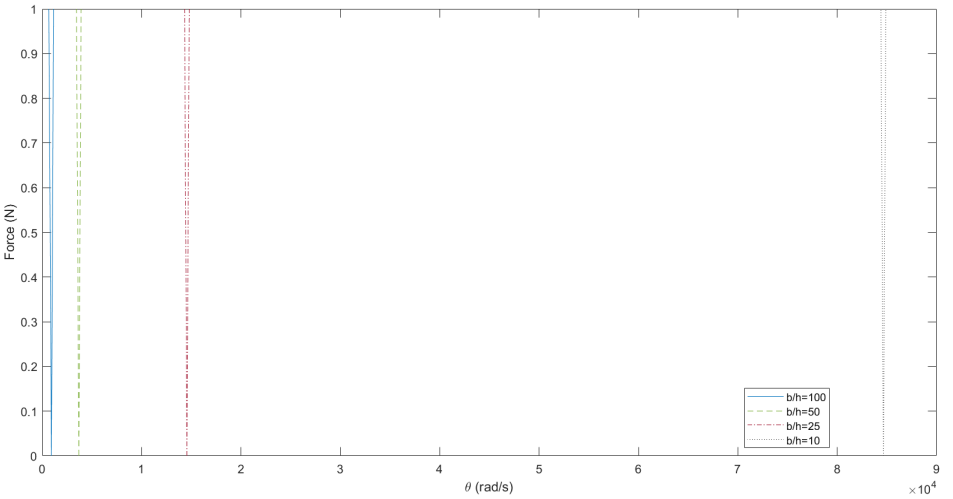

Figure 3.11: First dynamic instability region for different values of b/h

Conclusions

The results obtained for the orthotropic plate are in conformity with the ones found in the literature for both models and both approximations. All the relative deviations are lower than 1.5% and the majority

of them are lower than 1%. Once again, both models, FSDT and HSDT, presented equal or really similar results, as expected. For the orthotropic plate the literature presented results for the first and second approximation. As a consequence the relative deviations for the second approximation are not necessarily bigger than the ones obtained for the first approximation. Actually, for some points they are smaller.

Then, it is possible to conclude that the results obtained for an orthotropic square plate are in agreement with the ones found in the literature, even though their model formulate their system matrices resorting to the Rayleigh-Ritz method.

Finally, the results presented in Figure 3.11 allow to conclude that the ratio b/h has a great impact on the location of the principal dynamic instability region. The increase of b/h, meaning the decrease of the thickness, shifts the principal dynamic instability region to the left. So thicker plates have the instability regions in a zone of higher frequencies. The results also show that the difference is considerable since the difference on the frequencies of the boundaries are, sometimes, of some thousand rad/s.

3.4.3 Laminated Composite Plate

In this section, a four layer cross-ply laminated plate is analysed. Each ply has the same thickness and is a square plate with a [0°/90°/90°/0°] lay up, a ratio of $a/h = 25$ and $a = 10$in$= 0.254$m. Each ply was made of the same orthotropic material, which has the following mechanical properties: $E_2 = 10^6$lb/in$^2 = 6.8948$GPa, $E_1 = 40E_2$, $G_{12}/E_2 = G_{13}/E_2 = 0.6$, $G_{23}/E_2 = 0.5$, $\nu_{12} = 0.25$ and $\rho = 1$lbs^2/in$^4 = 1.06864 \times 10^7$kg/m^3.

Figure 3.12(a) and 3.12(b) depict, both approximations, of the principal dynamic instability region for the FSDT and HSDT model, respectively. The results are plotted as frequency θ (rad/s) against the dynamic load factor β.

The results obtained for the frequencies of the boundaries of the first instability region, for both models and both approximations, are presented in Table 3.9. Those results were compared with the ones indicated in Wang et al. [15], also shown in Table 3.9.

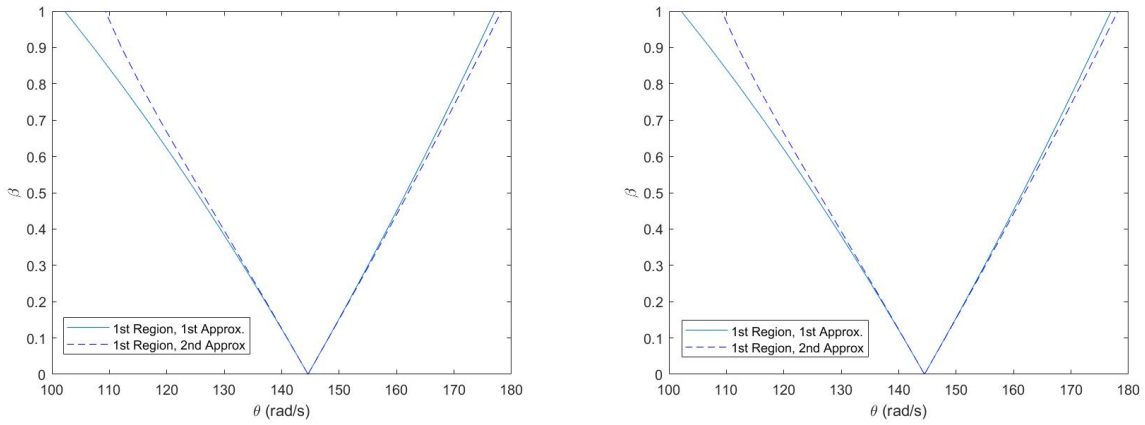

(a) using FSDT model

(b) using HSDT model

Figure 3.12: First and second approximation to principal region of dynamic instability for a four layered cross-ply laminated plate

Table 3.9: Frequency (rad/s) of the boundary of the first region of instability for a four layered cross-ply laminated plate

	FSDT				HSDT				Wang et al. [15]	
β	1^{st} Approx.		2^{nd} Approx.		1^{st} Approx.		2^{nd} Approx.			
	θ_1	θ_2	θ_1	θ_2	θ_1	θ_2	θ_1	θ_2	θ_1	θ_2
0	144.6	144.6	144.6	144.6	144.5	144.5	144.5	144.5	144.57	144.57
0.3	133.3	155	133.6	155.2	133.2	154.9	133.5	155.1	133.29	155.03
0.6	121	164.8	122.4	165.4	120.9	164.8	122.3	165.3	120.95	164.83
0.9	107.2	174.1	112.1	175.1	107.1	174	112	175	107.21	174.08

To better compare and analyse the results presented in the previous table, the relative deviations of the results obtained in this work and the ones presented in [15] were calculated and indicated in Table 3.10.

Table 3.10: Relative deviations of frequency θ_1 and θ_2 (%) for a four layered cross-ply laminated plate

	FSDT				HSDT			
β	1^{st} Approx.		2^{nd} Approx.		1^{st} Approx.		2^{nd} Approx.	
	θ_1	θ_2	θ_1	θ_2	θ_1	θ_2	θ_1	θ_2
0	0.02%	0.02%	0.02%	0.02%	0.05%	0.05%	0.05%	0.05%
0.3	0.01%	0.02%	0.23%	0.11%	0.07%	0.08%	0.16%	0.05%
0.6	0.04%	0.02%	1,20%	0.35%	0.04%	0.02%	1.12%	0.29%
0.9	0.01%	0.01%	4.56%	0.59%	0.10%	0.05%	4.47%	0.53%

Figure 3.13 depicts the two approximations for the first and second dynamic instability regions. As

done for the study of the orthotropic plate, the graph presented was obtained using the FSDT model since it presents a good accuracy and it is faster to compute than the HSDT.

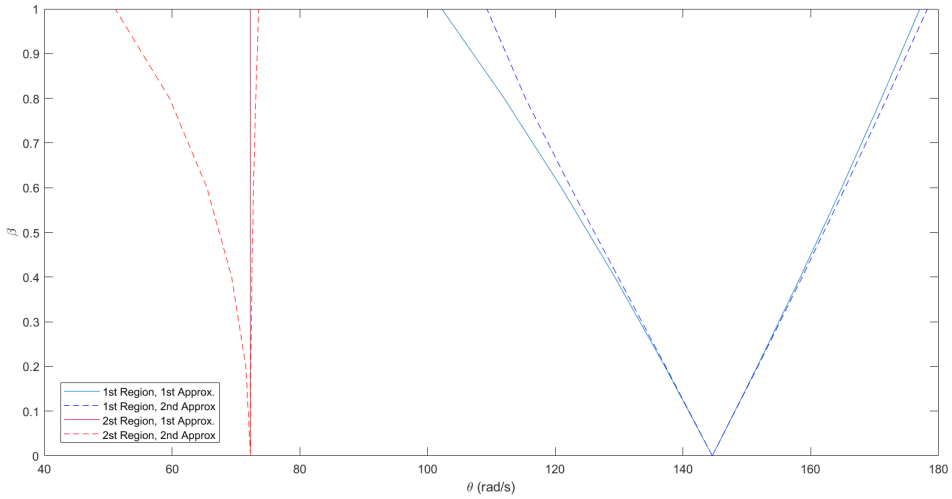

Figure 3.13: First and second approximation of the first and second dynamic instability region for a four layered cross-ply laminated plate

In order to understand how the ratio a/b affects the dynamic instability of a composite laminated plate a parametric study was performed. Analysing the same laminated composite plate already used in this section, but varying its relation a/b, the principal dynamic instability regions presented in Figure 3.14, were obtained.

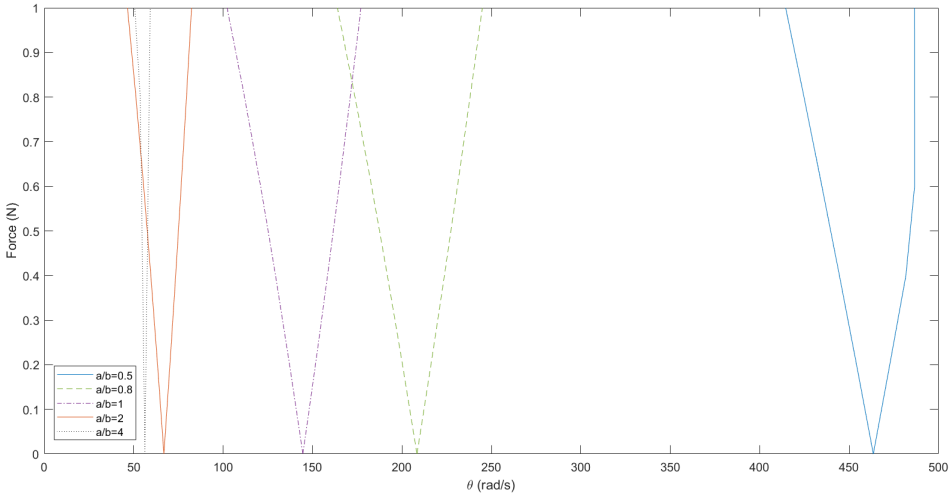

Figure 3.14: First dynamic instability region for different values of a/b

Conclusions

From the results obtained for the laminated composite plate, it is possible to conclude that the results obtained in this work are in accordance with the ones found in the literature. The relative deviations obtained are all lower than 5% and lower than 1.5% if not considering the point on the left boundary of

the second approximation for both FSDT and HSDT. Once again, and as expected, both theories, FSDT and HSDT, presented similar results for the frequencies of the boundaries of the instability dynamic region. Unfortunately, in the literature it was only found the results for the first approximation. Therefore the relative deviations for the second approximations were calculated comparing them to the ones of the first approximation of the literature. This can explain why the relative deviations for the second approximation are generally higher than the ones obtained for the first approximation.

At last, the parametric study show how the ratio a/b affects the dynamic instability region of a composite laminated plate. The results presented in Figure 3.14 permit to conclude that the decrease of a/b shifts the dynamic instability zone to the right, meaning to a zone with higher frequencies. The difference becomes less significant for higher ratios a/b and vice versa. The width of the region tends to decrease with the increase of a/b and, consequently, the area of the unstable dynamic region decreases with the increase of a/b.

Chapter 4

Sandwich Plates

In this chapter sandwich plates will be studied. The numerical model used to analyse them will be presented. A first validation of the model will be performed doing a free vibration analysis. Later on, the dynamic instability will be studied.

A special case of sandwich plates, where the core is made of a viscoelastic material, will be presented. It is already expectable that using this kind of materials in the core will add some kind of damping effect on the structure. A dynamic instability analysis will be performed and its effect will be studied.

4.1 Sandwich Plates

In this section it will be presented the formulation used to study a sandwich plate and its validation through a vibration analysis.

A sandwich panel generally consists of two thin but stiff face sheets or skins separated by a light-weight and thick but low modulus core [5]. A graphical representation of a sandwich panel can be seen in Figure 4.1.

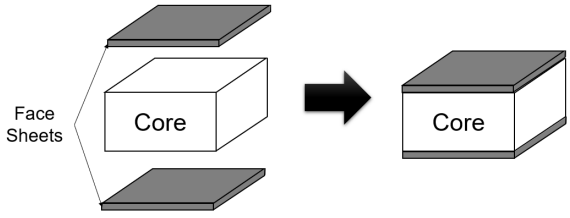

Figure 4.1: Sandwich Plate

The face sheets are usually laminated composite materials, but, can also be made of metallic materials. Moreover, the core is usually made of a light-weight material, such as, a foam polymer or a honeycomb material. The main objective of the core, in a sandwich plate, is to reduce the weight of the structure while producing a high resistance to transverse loads or damping unwanted vibrations.

It is, now, needed to develop a mathematical formulation that models sandwich plates in order to be able to proceed to different kinds of analyses and studies. The next subsection will present the models used in this work.

4.1.1 Numerical Model

As mentioned in section 1.3, the formulation used to study sandwich panels in this work is an adaptation and an expansion of the one developed by Tomé [32].

The model formulates the sandwich panel as two laminated composite plates (e_1, e_2) and an elastic core (c) between them. Figure 4.2 is a visual representation of the model developed.

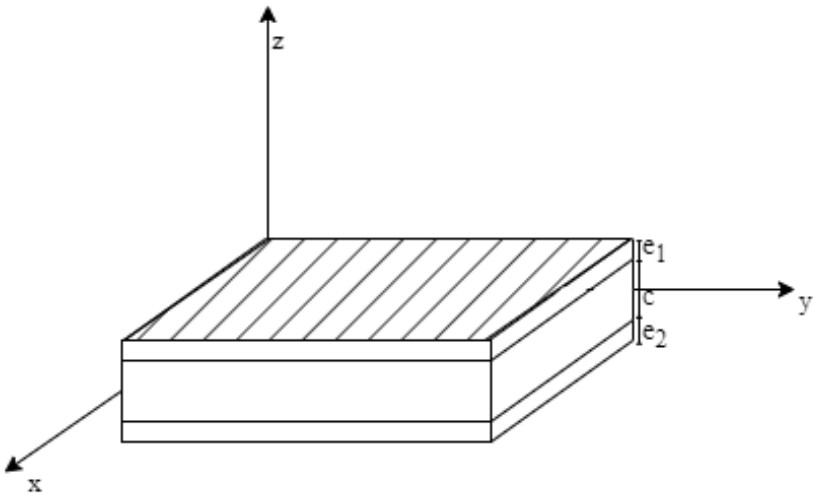

Figure 4.2: Sandwich plate model

The two laminated composite layers (e_1, e_2) are modelled using the first shear deformation theory (FSDT), while the core (c) is modelled with the higher-order shear deformation theory (HSDT).

The following assumptions are taken into account in the development of the sandwich panel model:

1. the origin of the z axis is the medium plane of the core layer;
2. no slip occurs at the interfaces between layers;
3. the displacements are continuous along the interfaces.

Adapting equations (2.16) for the laminated composite plates (e_1, e_2), the displacement field for these layers is given, in the general form, by:

$$u^i(x,y,z,t) = u_0^i(x,y,t) + (z - z_i)\,\theta_x^i(x,y,t) \tag{4.1a}$$

$$v^i(x,y,z,t) = v_0^i(x,y,t) + (z - z_i)\,\theta_y^i(x,y,t) \tag{4.1b}$$

$$w^i(x,y,z,t) = w_0^i(x,y,t) \tag{4.1c}$$

where $i = e_1, e_2$ and z_i is obtained by:

$$z_{e_1} = \frac{h_c}{2} + \frac{h_{e_1}}{2}, \qquad z_{e_2} = -\frac{h_c}{2} - \frac{h_{e_2}}{2} \tag{4.2}$$

Since the core is modelled with the HSDT, the displacement field is given adapting equation (2.25) and can be written as:

$$u_c\left(x,y,z,t\right) = u_0^c\left(x,y,t\right) + z\theta_x^c\left(x,y,t\right) + z^2 u_0^{*c}\left(x,y,t\right) + z^3\theta_x^{*c}\left(x,y,t\right) \tag{4.3a}$$

$$v^c\left(x,y,z,t\right) = v_0^c\left(x,y,t\right) + z\theta_y^c\left(x,y,t\right) + z^2 v_0^{*c}\left(x,y,t\right) + z^3\theta_y^{*c}\left(x,y,t\right) \tag{4.3b}$$

$$w^c\left(x,y,z,t\right) = w_0^c\left(x,y,t\right) + z\theta_z^c\left(x,y,t\right) + z^2 w_0^{*c}\left(x,y,t\right) \tag{4.3c}$$

Assumption 3 can be mathematically written as:

$$u^c = \left(x,y,\frac{h_c}{2},t\right) = u^{e_1}\left(x,y,\frac{h_c}{2},t\right), \qquad u^c = \left(x,y,-\frac{h_c}{2},t\right) = u^{e_2}\left(x,y,-\frac{h_c}{2},t\right) \tag{4.4a}$$

$$v^c = \left(x,y,\frac{h_c}{2},t\right) = v^{e_1}\left(x,y,\frac{h_c}{2},t\right), \qquad v^c = \left(x,y,-\frac{h_c}{2},t\right) = v^{e_2}\left(x,y,-\frac{h_c}{2},t\right) \tag{4.4b}$$

$$w^c = \left(x,y,\frac{h_c}{2},t\right) = w^{e_1}\left(x,y,t\right), \qquad w^c = \left(x,y,-\frac{h_c}{2},t\right) = w^{e_2}\left(x,y,t\right) \tag{4.4c}$$

Substituting these equations into the displacement field equations, (4.1) and (4.3), the following is obtained:

$$\theta_x^{e_1} = \frac{2}{h_{e_1}}\left(u_0^{e_1} - u_0^c - \frac{h_c}{2}\theta_x^c - \frac{h_c^2}{4}u_0^{*c} - \frac{h_c^3}{8}\theta_x^{*c}\right) \tag{4.5a}$$

$$\theta_x^{e_2} = \frac{2}{h_{e_2}}\left(-u_0^{e_2} + u_0^c - \frac{h_c}{2}\theta_x^c + \frac{h_c^2}{4}u_0^{*c} - \frac{h_c^3}{8}\theta_x^{*c}\right) \tag{4.5b}$$

$$\theta_y^{e_1} = \frac{2}{h_{e_1}}\left(v_0^{e_1} - v_0^c - \frac{h_c}{2}\theta_y^c - \frac{h_c^2}{4}v_0^{*c} - \frac{h_c^3}{8}\theta_y^{*c}\right) \tag{4.5c}$$

$$\theta_y^{e_2} = \frac{2}{h_{e_2}}\left(-v_0^{e_2} + v_0^c - \frac{h_c}{2}\theta_y^c + \frac{h_c^2}{4}v_0^{*c} - \frac{h_c^3}{8}\theta_y^{*c}\right) \tag{4.5d}$$

$$\theta_z^c = \frac{w_0^{e_1} - w_0^{e_2}}{h_c}, \qquad w_0^{*c} = \frac{4}{h_c^2}\left(\frac{w_0^{e_1} + w_0^{e_2}}{2} - w_0^c\right) \tag{4.5e}$$

As done before in section 2.2, the linear and non-linear strains are obtained by substituting the respective displacement field into equations (2.18) and (2.19), the linear and non linear strain-displacement relations, respectively.

Therefore, for the laminated composite plates layers e_1 and e_2, the linear and non-linear strains are given substituting equations (4.1) into equations (2.18) and (2.19), respectively. The non zero linear terms are, then, written as:

$$
\begin{aligned}
\varepsilon_{xx}^{i\ L} &= \frac{\partial u_0^i}{\partial x} + (z - z_i)\frac{\partial \theta_x^i}{\partial x} = \varepsilon_{xx}^{i\ (0)} + z\kappa_{xx}^{i\ (1)} \\
\varepsilon_{yy}^{i\ L} &= \frac{\partial v_0^i}{\partial y} + (z - z_i)\frac{\partial \theta_y^i}{\partial y} = \varepsilon_{yy}^{i\ (0)} + z\kappa_{yy}^{i\ (1)} \\
\gamma_{xy}^{i\ L} &= \left(\frac{\partial u_0^i}{\partial y} + \frac{\partial v_0^i}{\partial x}\right) + (z - z_i)\left(\frac{\partial \theta_x^i}{\partial y} + \frac{\partial \theta_y^i}{\partial x}\right) = \gamma_{xy}^{i\ (0)} + z\kappa_{xy}^{i\ (1)} \\
\gamma_{yz}^{i\ L} &= \theta_y^i + \frac{\partial w_0^i}{\partial y} = \gamma_{yz}^{i\ (0)} \\
\gamma_{xz}^{i\ L} &= \theta_x^i + \frac{\partial w_0^i}{\partial x} = \gamma_{xz}^{i\ (0)}
\end{aligned}
\tag{4.6}
$$

where $i = e_1, e_2$.

The following vectors group these variables regarding their contribution to membrane (m), bending(b) and shear (s).

$$
\{\varepsilon_m^i\} = \begin{Bmatrix} \varepsilon_{xx}^{i\ (0)} \\ \varepsilon_{yy}^{i\ (0)} \\ \gamma_{xy}^{i\ (0)} \end{Bmatrix}, \qquad \{\varepsilon_b^i\} = \begin{Bmatrix} \kappa_{xx}^{i\ (1)} \\ \kappa_{yy}^{i\ (1)} \\ \kappa_{xy}^{i\ (1)} \end{Bmatrix} \qquad \{\varepsilon_s^i\} = \begin{Bmatrix} \gamma_{yz}^{i\ (0)} \\ \gamma_{xz}^{i\ (0)} \end{Bmatrix}, \tag{4.7}
$$

On the other hand, for the core (c), the linear and non-linear strains are given substituting equations (4.3) into equations (2.18) and (2.19), respectively. Thus, the linear strain terms can be given by:

$$
\begin{aligned}
\varepsilon_{xx}^{c\ L} &= \frac{\partial u_0^c}{\partial x} + z\frac{\partial \theta_x^c}{\partial x} + z^2\frac{\partial u_0^{*c}}{\partial x} + z^3\frac{\partial \theta_x^{*c}}{\partial x} = \varepsilon_{xx}^{c\ (0)} + z\kappa_{xx}^{c\ (1)} + z^2\varepsilon_{xx}^{c\ (2)} + z^3\kappa_{xx}^{c\ (3)} \\
\varepsilon_{yy}^{c\ L} &= \frac{\partial v_0^c}{\partial y} + z\frac{\partial \theta_y^c}{\partial y} + z^2\frac{\partial v_0^{*c}}{\partial y} + z^3\frac{\partial \theta_y^{*c}}{\partial y} = \varepsilon_{yy}^{c\ (0)} + z\kappa_{yy}^{c\ (1)} + z^2\varepsilon_{yy}^{c\ (2)} + z^3\kappa_{yy}^{c\ (3)} \\
\varepsilon_{zz}^{c\ L} &= \theta_z^c + 2zw_0^{*c} = \varepsilon_{zz}^{c\ (0)} + z\kappa_{zz}^{c\ (1)} \\
\gamma_{yz}^{c\ L} &= \left(\theta_y^c + \frac{\partial w_0^c}{\partial y}\right) + z\left(2v_0^{*c} + \frac{\partial \theta_z^c}{\partial y}\right) + z^2\left(3\theta_y^{*c} + \frac{\partial w_0^{*c}}{\partial y}\right) = \gamma_{yz}^{c\ (0)} + z\kappa_{yz}^{c\ (1)} + z^2\gamma_{yz}^{c\ (2)} \\
\gamma_{xz}^{c\ L} &= \left(\theta_x^c + \frac{\partial w_0^c}{\partial x}\right) + z\left(2u_0^{*c} + \frac{\partial \theta_z^c}{\partial x}\right) + z^2\left(3\theta_x^{*c} + \frac{\partial w_0^{*c}}{\partial x}\right) = \gamma_{xz}^{c\ (0)} + z\kappa_{xz}^{c\ (1)} + z^2\gamma_{xz}^{c\ (2)} \\
\gamma_{xy}^{c\ L} &= \left(\frac{\partial u_0^c}{\partial y} + \frac{\partial v_0^c}{\partial x}\right) + z\left(\frac{\partial \theta_x^c}{\partial y} + \frac{\partial \theta_y^c}{\partial x}\right) + z^2\left(\frac{\partial u_0^{*c}}{\partial y} + \frac{\partial v_0^{*c}}{\partial x}\right) + z^3\left(\frac{\partial \theta_x^{*c}}{\partial y} + \frac{\partial \theta_y^{*c}}{\partial x}\right) = \\
&\qquad \gamma_{xy}^{c\ (0)} + z\kappa_{xy}^{c\ (1)} + z^2\gamma_{xy}^{c\ (2)} + z^3\kappa_{xy}^{c\ (3)}
\end{aligned}
\tag{4.8}
$$

The following vectors group these variables regarding their contribution to membrane (m), bending(b) and shear (s).

$$\{\varepsilon_m^c\} = \begin{Bmatrix} \varepsilon_{xx}^{c\ (0)} \\ \varepsilon_{yy}^{c\ (0)} \\ \gamma_{xy}^{c\ (0)} \\ \varepsilon_{xx}^{c\ (2)} \\ \varepsilon_{yy}^{c\ (2)} \\ \gamma_{xy}^{c\ (2)} \\ \varepsilon_{zz}^{c\ (0)} \end{Bmatrix}, \qquad \{\varepsilon_b^c\} = \begin{Bmatrix} \kappa_{xx}^{c\ (1)} \\ \kappa_{yy}^{c\ (1)} \\ \kappa_{xy}^{c\ (1)} \\ \kappa_{xx}^{c\ (3)} \\ \kappa_{yy}^{c\ (3)} \\ \kappa_{xy}^{c\ (3)} \\ \kappa_{zz}^{c\ (1)} \end{Bmatrix} \qquad \{\varepsilon_s^c\} = \begin{Bmatrix} \gamma_{yz}^{c\ (0)} \\ \gamma_{xz}^{c\ (0)} \\ \gamma_{yz}^{c\ (2)} \\ \gamma_{xz}^{c\ (2)} \\ \kappa_{yz}^{c\ (1)} \\ \kappa_{xz}^{c\ (1)} \end{Bmatrix}, \tag{4.9}$$

The finite element model used to study sandwich plates is an eight-node serendipity quadratic model, as presented in section 2.3, but with 15 degrees of freedom per node. In these 15 degrees of freedom, the first and last three are regarding the top and bottom laminated composited face sheets, respectively, and the 11 in between are regarding the core (c).

This change won't affect the process and calculations already presented in section 2.3. Although it will cause changes on some vectors and matrices. The vector of nodal degrees of freedom of the sandwich plate, $\{d_i^e\}$, corresponding to node i, assumes the following form:

$$\begin{aligned} \{d_i^e\} = \{&(u_0^{e_2})_i^e \quad (v_0^{e_2})_i^e \quad (w_0^{e_2})_i^e \quad (u_0^c)_i^e \quad (v_0^c)_i^e \quad (w_0^c)_i^e \quad (\theta_x^c)_i^e \quad \left(\theta_y^c\right)_i^e \quad ... \\ &... \quad (u_0^{*c})_i^e \quad (v_0^{*c})_i^e \quad (\theta_x^{*c})_i^e \quad \left(\theta_y^{*c}\right)_i^e \quad (u_0^{e_1})_i^e \quad (v_0^{e_1})_i^e \quad (w_0^{e_1})_i^e\} \end{aligned} \tag{4.10}$$

The matrix $[Z]$, essential to obtain the mass matrix, will present the following form:

$$[Z] = \begin{bmatrix} 1-(z-z_{e_2})\frac{2}{h_{e_2}} & 0 & 0 \\ 0 & 1-(z-z_{e_2})\frac{2}{h_{e_2}} & 0 \\ 0 & 0 & 1-\frac{z}{h_c}+z^2\frac{4}{h_c^2} \\ 1+\frac{2}{h_{e_2}}(z-z_{e_2})-\frac{2}{h_{e_1}}(z-z_{e_1}) & 0 & 0 \\ 0 & 1+\frac{2}{h_{e_2}}(z-z_{e_2})-\frac{2}{h_{e_1}}(z-z_{e_1}) & 0 \\ 0 & 0 & 1-z^2\frac{4}{h_c^2} \\ z-\frac{h_c}{h_{e_2}}(z-z_{e_2})-\frac{h_c}{h_{e_1}}(z-z_{e_1}) & 0 & 0 \\ 0 & z-\frac{h_c}{h_{e_2}}(z-z_{e_2})-\frac{h_c}{h_{e_1}}(z-z_{e_1}) & 0 \\ z^2+\frac{h_c^2}{2h_{e_2}}(z-z_{e_2})-\frac{h_c^2}{2h_{e_1}}(z-z_{e_1}) & 0 & 0 \\ 0 & z^2+\frac{h_c^2}{2h_{e_2}}(z-z_{e_2})-\frac{h_c^2}{2h_{e_1}}(z-z_{e_1}) & 0 \\ z^3-\frac{h_c^3}{4h_{e_2}}(z-z_{e_2})-\frac{h_c^3}{4h_{e_1}}(z-z_{e_1}) & 0 & 0 \\ 0 & z^3-\frac{h_c^3}{4h_{e_2}}(z-z_{e_2})-\frac{h_c^3}{4h_{e_1}}(z-z_{e_1}) & 0 \\ 1+\frac{2}{h_{e_1}}(z-z_{e_1}) & 0 & 0 \\ 0 & 1+\frac{2}{h_{e_1}}(z-z_{e_1}) & 0 \\ 0 & 0 & 1+\frac{z}{h_c}+z^2\frac{4}{h_c^2} \end{bmatrix}^T \tag{4.11}$$

Besides that, the auxiliary vector $\{G^{'}\}_k$, used to obtained the geometric stiffness matrix, for each

layer $k = e_1, e_2, c$, is now written as:

$$\{G^{'}\}_k = \sum_{i=1}^{8} [G_i^k]\{d_i^e\} \tag{4.12}$$

$$\{G'\}_{k=e_1,e_2} = \{\theta_x^k \quad \theta_y^k \quad \frac{\partial u_0^k}{\partial x} \quad \frac{\partial u_0^k}{\partial y} \quad \frac{\partial v_0^k}{\partial x} \quad \frac{\partial v_0^k}{\partial y} \quad \frac{\partial w_0^k}{\partial x} \quad \frac{\partial w_0^k}{\partial y} \quad -z_i\frac{\partial \theta_x^k}{\partial x} \quad -z_i\frac{\partial \theta_x^k}{\partial y} \quad ... \\ ... \quad -z_i\frac{\partial \theta_y^k}{\partial x} \quad -z_i\frac{\partial \theta_y^k}{\partial y}\frac{\partial \theta_x}{\partial x}\frac{\partial \theta_x}{\partial y}\frac{\partial \theta_y}{\partial x}\frac{\partial \theta_y}{\partial y}\}^T \tag{4.13}$$

$$\{G'\}_c = \{\theta_x^c \quad \theta_y^c \quad \theta_z^c \quad 2u_0^{*c} \quad 2v_0^{*c} \quad 2w_0^{*c} \quad 3\theta_x^{*c} \quad 3\theta_y^{*c} \quad \frac{\partial u_0^c}{\partial x} \quad \frac{\partial u_0^c}{\partial y} \quad \frac{\partial v_0^c}{\partial x} \quad \frac{\partial v_0^c}{\partial y} \quad \frac{\partial w_0^c}{\partial x} \quad \frac{\partial w_0^c}{\partial y} \quad \frac{\partial \theta_x^c}{\partial x} \quad \frac{\partial \theta_x^c}{\partial y} \\ \frac{\partial \theta_y^c}{\partial x} \quad \frac{\partial \theta_y^c}{\partial y} \quad \frac{\partial \theta_z^c}{\partial x} \quad \frac{\partial \theta_z^c}{\partial y} \quad \frac{\partial u_0^{*c}}{\partial x} \quad \frac{\partial u_0^{*c}}{\partial y} \quad \frac{\partial v_0^{*c}}{\partial x} \quad \frac{\partial v_0^{*c}}{\partial y} \quad \frac{\partial w_0^{*c}}{\partial x} \quad \frac{\partial w_0^{*c}}{\partial y} \quad \frac{\partial \theta_x^{*c}}{\partial x} \quad \frac{\partial \theta_x^{*c}}{\partial y} \quad \frac{\partial \theta_y^{*c}}{\partial x} \quad \frac{\partial \theta_y^{*c}}{\partial y}\}^T \tag{4.14}$$

4.1.2 Vibration Analysis

Building the stiffness matrix $[K]$ and the mass matrix $[M]$ of a sandwich plate, using the model presented in the previous section, it is possible to obtain its natural frequencies. As before, this can be achieved performing the eigenvalue problem at equation (2.59).

The plate considered in this analysis is simply supported in all four edges. Table 4.1 indicates the details of the boundary conditions applied in the sandwich plate.

Table 4.1: Details of boundary conditions used on the vibration analysis for a sandwich plate

	Top Face Sheet	Core	Bottom Face Sheet
$x = 0, a$	$v_0 = w_0 = 0$	$v_0 = w_0 = \theta_y = v_0^* = \theta_y^* = 0$	$v_0 = w_0 = 0$
$y = 0, b$	$u_0 = w_0 = 0$	$u_0 = w_0 = \theta_x = u_0^* = \theta_x^* = 0$	$u_0 = w_0 = 0$

The plate studied in this section was a square sandwich plate with a [0°/90°/0°/core/0°/90°/0°] lay up, $a/h = 10$ and $h_c/h = 0.88$. The face sheets were made of glass polyester resins, having the following properties: $E_1 = 24.51$GPa, $E_2 = 7.77$GPa, $G_{12} = G_{13} = 3.34$GPa, $G_{23} = 1.34$GPa, $\nu_s = 0.078$ and $\rho_s = 0.078$Kg/m^3. The core material was HEREX C70.130 PVC foam, which has the following mechanical properties: $E_c = 103.63$MPa, $G_c = 50$MPa, $\nu_c = 0.32$ and $\rho_c = 130$Kg/m^3.

Table 4.2 present the results obtained and the comparision with the ones presented in Nayak et al. [23]. The non dimensional natural frequencies are given by:

$$\bar{\omega} = \omega\frac{a^2}{h}\sqrt{\frac{\rho_c}{E_c}} \tag{4.15}$$

Table 4.2: Non dimensional free vibration frequency results for a sandwich plate

Mode	Mesh $N \times N$	$\bar{\omega}$ Present Model	$\bar{\omega}$ Nayak et al.[23]	Relative error
(1,1)	2x2	14.69	15.04	2.33%
	5x5	14.42	15.04	4.12%
	10x10	14.46	15.04	3.86%
	15x15	14.52	15.04	3.46%
	20x20	14.60	15.04	2.93%
(1,2)	2x2	31.91	28.10	13.56%
	5x5	26.65	28.10	5.16%
	10x10	26.62	28.10	5.27%
	15x15	26.64	28.10	5.20%
	20x20	26.67	28.10	5.09%
(2,1)	2x2	32.56	29.20	11.51%
	5x5	27.28	29.20	6.58%
	10x10	27.25	29.20	6.68%
	15x15	27.26	29.20	6.64%
	20x20	27.28	29.20	6.58%
(2,2)	2x2	40.98	37.76	8.53%
	5x5	35.44	37.76	6.14%
	10x10	35.36	37.76	6.36%
	15x15	35.37	37.76	6.33%
	20x20	35.38	37.76	6.30%

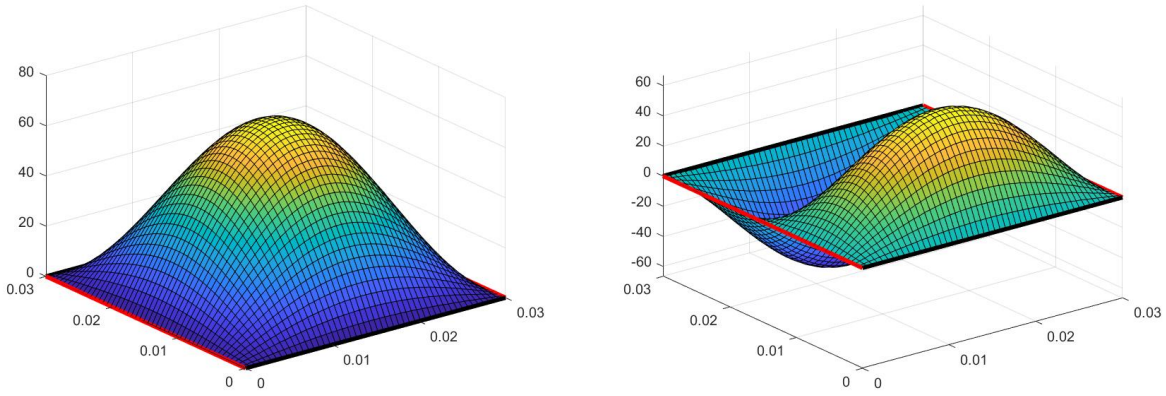

(a) Mode (1,1)

(b) Mode (1,2)

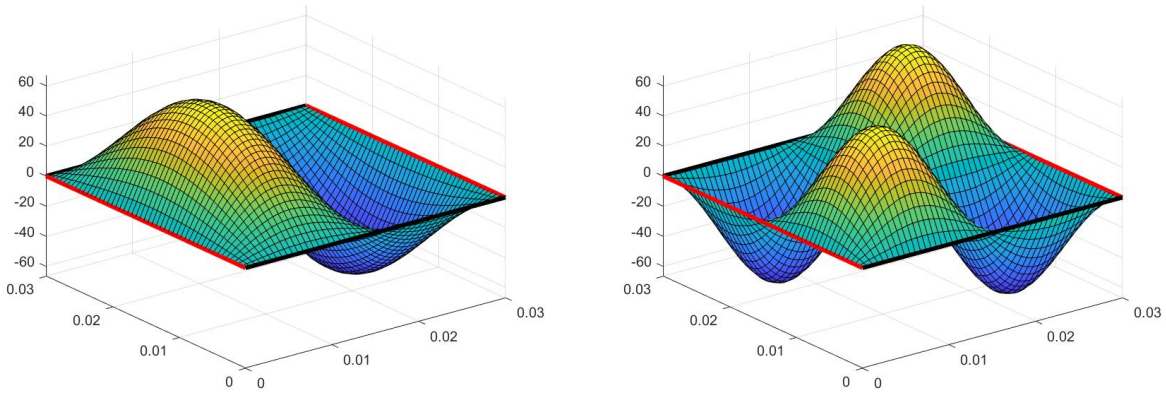

(c) Mode (2,1)

(d) Mode (2,2)

Figure 4.3: Vibration Modes of a sandwich plate

Regarding convergence, it is possible to say that the results converge early on, after a mesh size of 5×5 or 10×10 for all modes studied. Relevant to mention that, for the first mode, even though, the smallest relative error is for a mesh size of 2×2, the error gets smaller with the increase of the mesh size after 2×2. Results for a mesh size bigger than 20×20 would presented a smaller error, but due to the computational and memory effort required it was not possible to obtained them.

It is possible to conclude that, although the results have errors higher than 2%, and for some modes, higher than 5%, when compared with the ones obtained in [23], they are still good results. Once there are no errors higher than 10%, the results obtained validate the formulations of the mass matrix and stiffness matrix for a sandwich plate. This discrepancy can be explained by the different models used to obtained these results. In the present work the sandwich plate is modelled using an eight-node serendipity quadratic element and the FSDT for the face sheets and the HSDT for the core. Instead, in [23], to obtain the results used to do the comparison the formulation of the sandwich plate is made using a ESL model and Reddy's higher order theory but a 9 node quadratic element.

4.1.3 Dynamic Instability Analysis

To study the dynamic instability of a sandwich plate using the model just presented in section 4.1.1, a five layered square symmetric sandwich plate was analysed. The plate consists of laminated cross ply face sheets and an isotropic core with a [0°/90°/core/90°/0°] lay up. Each of the face sheet plies is assumed to be the same thickness, the ratio between the thickness of the core and the total thickness (h_c/h) is taken to be 0.8, being the total thickness 1mm, and the ratio a/h is 10. The properties of the materials used for the face sheets and the core are the following:

- Face sheets: $E_1 = 276$GPa, $E_2 = G_{12} = G_{13} = G_{23} = 10.34$GPa, $\nu_{12} = 0.22$ and $\rho = 681.8$Kg/m^3;
- $E_1 = E_2 = 0.5776$GPa, $G_{12} = G_{13} = 0.1079$GPa, $G_{23} = 0.22215$GPa, $\nu_{12} = 0.0025$ and $\rho = 1000$kg/m^3.

Figure 4.4 depicts the principal dynamic instability region for both, the first and second, approximations.

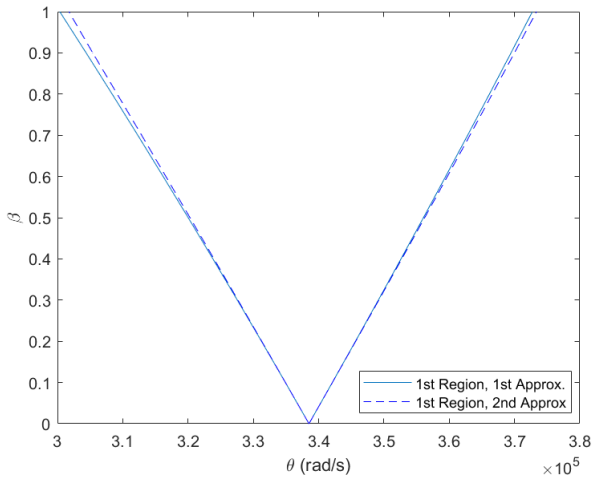

Figure 4.4: First and second approximation of the first dynamic instability region for a symmetric sandwich plate

Table 4.3 presents the non-dimensional excitation frequencies of the boundary of the instability region obtained for the first and second approximations. The same table, also, indicates the non-dimensional results exhibit in Sahoo et al. [27], which uses a hyperbolic zigzag theory to model the plates. It is important to mention that these values were obtained from the graph presented in [27], which can lead to some lack of accuracy between the exact values obtained in [27] and the ones presented in Table 4.3. The non-dimensional frequencies were obtained by:

$$\bar{\theta} = 100\theta a\sqrt{\frac{\rho_c}{E_{1f}}} \tag{4.16}$$

where ρ_c is the densidity of the core and E_{1f} is the Young's modulus of the face sheets.

Table 4.3: Non-dimensional frequency of the boundary of the first region of instability for a symmetric sandwich plate

β	Present				Sahoo et al. [27]	
	1^{st} Approx.		2^{nd} Approx.			
	$\bar{\theta_1}$	$\bar{\theta_2}$	$\bar{\theta_1}$	$\bar{\theta_2}$	$\bar{\theta_1}$	$\bar{\theta_2}$
0	20.375	20.375	20.375	20.375	19.674	19.674
0.2	19.936	20.803	19.942	20.809	19.110	20.223
0.4	19.491	21.224	19.503	21.230	18.516	20.742
0.6	19.033	21.633	19.057	21.651	17.923	21.276

To make it easier to compare the results obtained with the model presented in this work and the results presented in [27], Table 4.4 indicates the relative deviations between both results.

Table 4.4: Relative deviations of non-dimensional frequency $\bar{\theta_1}$ and $\bar{\theta_2}$ (%) for a symmetric sandwich plate

β	1^{st} Approx.		2^{nd} Approx.	
	$\bar{\theta_1}$	$\bar{\theta_2}$	$\bar{\theta_1}$	$\bar{\theta_2}$
0	3.56%	3.56%	3.56%	3.56%
0.2	4.32%	2.87%	4.35%	2.90%
0.4	5.27%	2.32%	5.33%	2.35%
0.6	6.19%	1.68%	6.33%	1.76%

Figure 4.5 depicts the first and second approximations for both, the first and second dynamic instability regions, for the plate under analysis in this section.

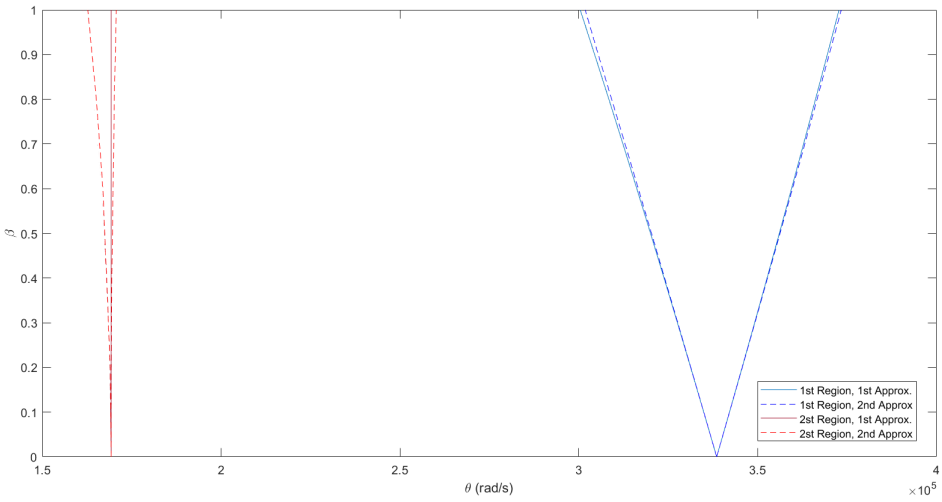

Figure 4.5: First and second approximation of the first and second dynamic instability region for a symmetric sandwich plate

The core and its dimensions is a relevant part of a sandwich plate and it will have an important impact on the mechanical behaviour of the plate. In order to study the influence of the thickness of the core on the dynamic instability of a sandwich plate, the principal dynamic instability region was obtained, for the sandwich plate already studied in this section, for different values of h_c/h. Figure 4.6 depicts the results obtained.

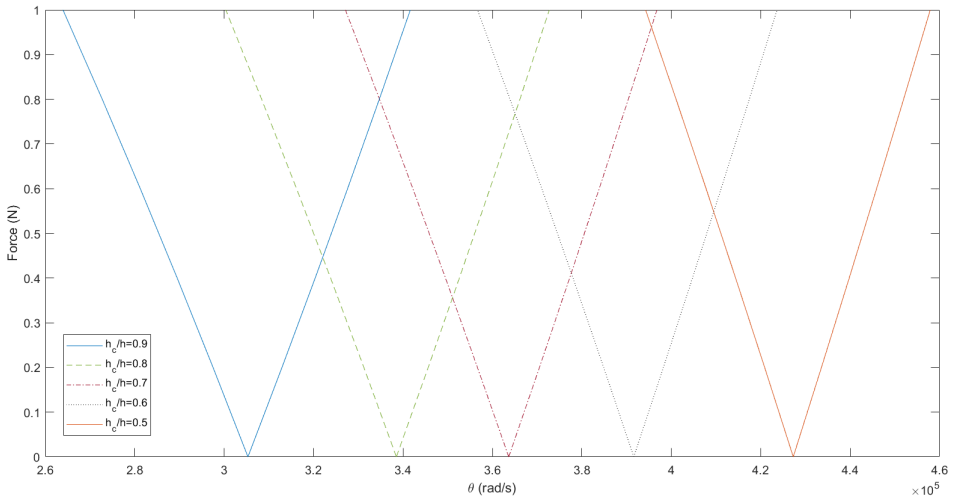

Figure 4.6: First dynamic instability region for different values of h_c/h

Conclusions

The results obtained for the sandwich plate are not as close to the results found in the literature as the plates previously studied. However the relative deviations are lower than 10%. As already mention, the values from the literature were obtained using a graph from [27] which can bring some imprecision to the results used in the comparison. Besides that, [27] used a different element in the FEM and instead of the Bolontin's method to obtain the dynamic instability regions, they applied a different method developed by themselves. These can explain some of the discrepancies obtained between the results. Although it is not used to build the graph from Figure 4.4 the point in the right boundary of the second approximation for $\beta = 0.8$ presents a jump which clearly means that its calculation has a numerical and computational error associated.

However, at the end, one can say that the results obtained in this work are validated by the ones found in literature since its relative deviations are lower than 10% and some of them lower than 5%.

The last analysis, whose results are presented on Figure 4.6, shows that the decrease of the ratio h_c/h shifts the principal dynamic instability region to the right. This means that sandwich plates with thicker cores will have the principal dynamic instability region for lower frequencies and vice versa.

4.2 Sandwich Plates with Viscoelastic Core

In this section two numerical models that can be used to describe the mechanical behaviour of a sandwich plate with a viscoelastic core will be presented.

The material that composes the core will have a big influence on the mechanical behaviour of the sandwich plate. Because of that, it is extremely important to choose an appropriate material. Some materials are more advantageous than others, including, most especially, viscoelastic materials.

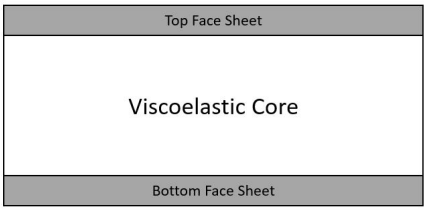

Figure 4.7: Sandwich plate with a viscoelastic core

Viscoelastic materials are frequently employed as core materials where damping is a major concern because they undergo significant deformations under external pressure and have the capacity to absorb and dissipate energy. They have characteristics of both viscous and elastic materials. The damping effect can be added to the model in different ways. In this work it is going to be used two different types of damping, proportional damping and hysteretic damping, which uses complex variables.

4.2.1 Proportional Damping

Considering the equation of motion of a plate, already shown on equation (3.1c), it can be added a damping term as follows:

$$[M]\{\ddot{x}\} + [C]\{\dot{x}\} + [K]\{x\} - P(t)[K_G]\{x\} = 0 \tag{4.17}$$

where [C] is the damping matrix in the form $[C] = \alpha[M] + \beta[K]$ but, during the development of this work, $\beta = 0$ was considered. If the damping coefficient (ϵ) is given by $\epsilon = \alpha/2$ the following can be done:

$$e^{-\epsilon t} = I + \sum_{k=1}^{\infty} \frac{\epsilon^k (-t)^k}{k!} \tag{4.18}$$

Equation (4.17) leads to the following form, when the solutions are in the form $x = e^{-\epsilon t}u(t)$ and $e^{-\epsilon t}$ is not singular:

$$[K]^{-1}[M]\{\ddot{u}\} + \{[I] - [K]^{-1}[M]\epsilon^2 - [P_s + P_d\phi(t)]\,[K]^{-1}[K_G]\}\{u\} = 0 \tag{4.19}$$

Extending the considerations given in section 3.2, it is easy to conclude that the boundary of the dynamic instability regions is given by the periodic solutions with period T and 2T. The boundary frequency equations can be also found by looking for periodic solutions, such as the Fourier series represented by equations (3.2) and (3.3), which, when inserted into equation (4.17), offer two linear homogeneous

systems with approximate solutions. Equation (4.20) presents the system to obtained solutions with a period of 2T.

$$\begin{vmatrix} [I] - (P_S + \frac{P_d}{2})[K]^{-1}[K_G] - \frac{\theta^2}{4}[K]^{-1}[M] & -\theta[K]^{-1}[M]\epsilon \\ \theta[K]^{-1}[M]\epsilon & [I] - (P_S + \frac{P_d}{2})[K]^{-1}[K_G] - \frac{\theta^2}{4}[K]^{-1}[M] \end{vmatrix} = 0 \quad (4.20)$$

4.2.2 Hysteretic Damping

As already mentioned, the hysteretic damping can be added to the system through the use of complex variable. The shear modulus of viscoelastic materials is expressed in complex form as:

$$G = G' + iG'' \quad (4.21)$$

where G' and G" are the real part and imaginary part of the complex modulus and are measures of the total energy stored and dissipated, respectively.

In this work to modelled a sandwich plate with viscoelastic core, it was used the model already presented in section 4.1.1, giving complex values for the Young's modulus. Then E can be written as:

$$E_c = E' + \eta E' i \quad (4.22)$$

where η is the material loss factor. This will lead to complex values in the matrices of the system, including the stiffness matrix and geometric stiffness matrix. The analysis performed is done using exactly the same model presented in sections 3.2 and 2.4 to obtain the dynamic instability regions and natural frequencies, respectively. The results obtained from the eigenvalue problems will be, obviously, complex and it will be needed to calculate their modulus to obtain the final result.

For sandwich plates with a viscoelastic core the vibration characteristics are usually associated with the modal loss factor. The measure of the vibratory energy absorbed by the structure is represented by the modal loss factors, which are the normalised imaginary portions of the bending stiffness. Therefore, it is important to obtain this factor for a better understanding of the plate. The modal loss factor can be calculated by:

$$\eta_i = \frac{\omega_I}{\omega_R} \quad (4.23)$$

where i indicates the mode, ω_I is the imaginary component of ω and ω_R is the real part.

4.2.3 Dynamic Instability Analysis - Results

To analyse the effects of adding a viscoelastic core to a sandwich plate the same plate was studied for both methods. The plate under analysis is a square, three layered sandwich plate with a [0°/core/0°] lay-up, thickness of 1mm and $a/h = 100$. The mechanical properties of the isotropic materials that the face sheet and the core are made of are the following:

- Face sheets: $E_f = 66$GPa, $\nu_{12} = 0.33$ and $\rho_f = 2680$Kg/m^3;

- Core: $E_c = 5.2 + \eta 5.2i$MPa, $\nu_{12} = 0.3$ and $\rho_c = 1015$Kg/m^3.

Proportional Damping

To better understand the effect of the viscoelastic core, Figure 4.8 depicts the principal dynamic instability region for the sandwich plate with $\alpha = 0$, meaning that it should behave like a system without damping, therefore a purely elastic core. Whereas, Figure 4.9 presents the same region for a sandwich plate with a viscoelastic core with $\alpha = 50$.

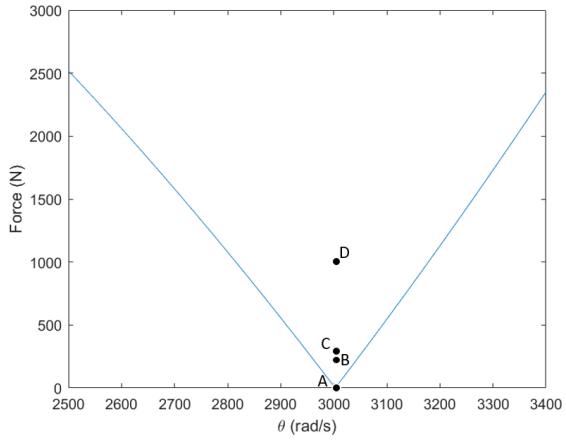

Figure 4.8: Principal dynamic instability region for $\alpha = 0$

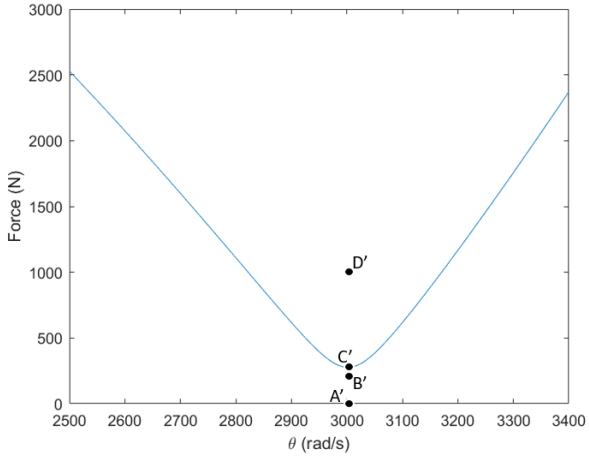

Figure 4.9: Principal dynamic instability region for $\alpha = 50$

In order to analyse the effect that damping has on the behaviour of the plate over time a direct integration using Newmark's Method was performed. The time increment used was $\Delta t = 0.00008$s and an initial displacement of 0.0004m was imposed to the w_0 degree of freedom on the central node of the plate. A group of the same load cases were studied for both plates to better compare the damping effect on different regions. The load cases studied are presented in Table 4.5 and its location on the dynamic instability region can be seen in Figures 4.8 and 4.9. Figures 4.10(a-d) depict the time vs. displacement diagrams for the load cases for $\alpha = 0$ and Figures 4.11(a-d) for $\alpha = 50$.

Table 4.5: Load cases used to obtain the displacement vs time diagrams

Points	θ (rad/s)	P_d (N)
A and A'	3002	0
B and B'	3003	200
C and C'	3002	216.3
D and D'	3002	1000

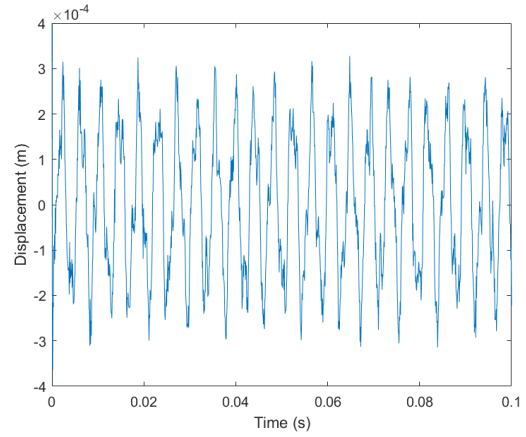

(a) Point A

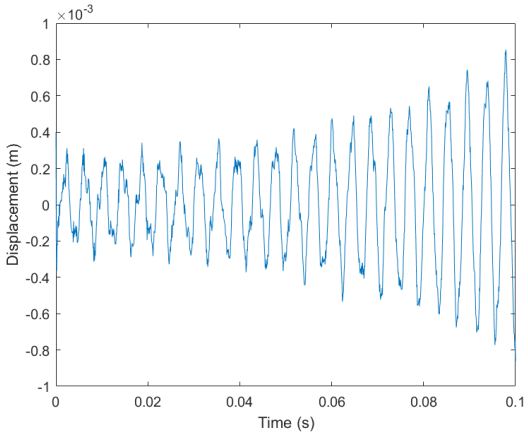

(b) Point B

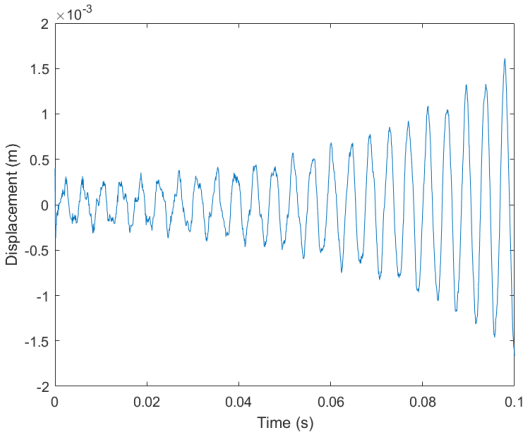

(c) Point C

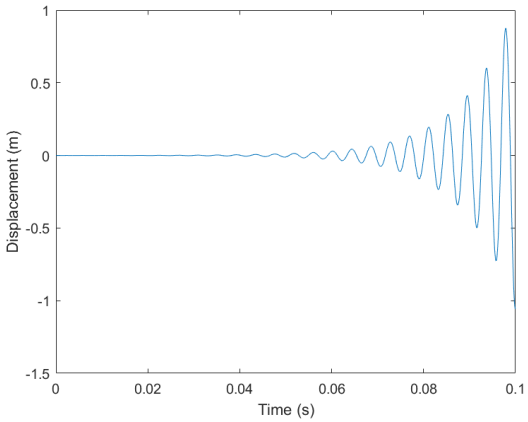

(d) Point D

Figure 4.10: Displacement vs Time diagrams of a sandwich plate with a purely elastic core with $\alpha = 0$

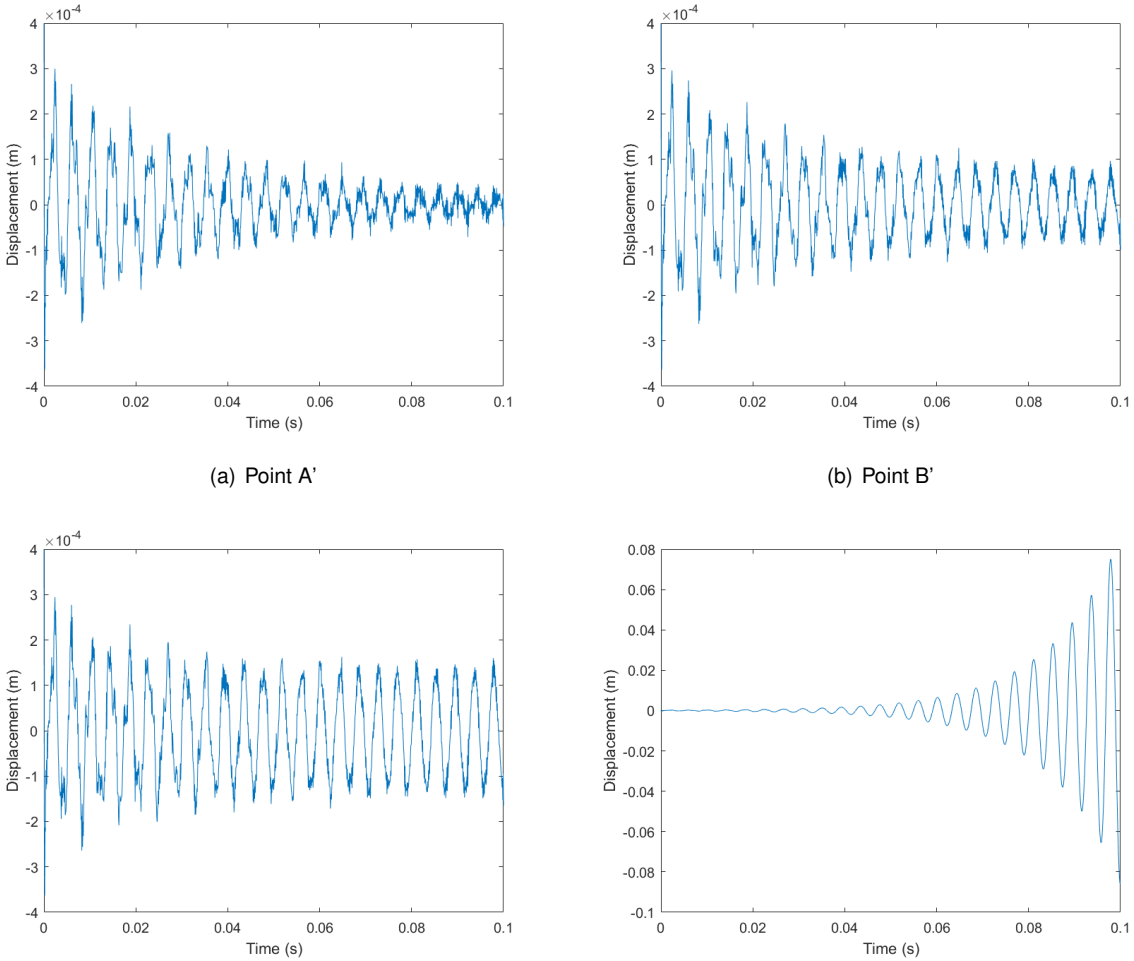

(a) Point A'

(b) Point B'

(c) Point C'

(d) Point D'

Figure 4.11: Displacement vs Time diagrams of a sandwich plate with viscoelastic core with $\alpha = 50$

To study the effect of α on the mechanical behaviour and, consequently, on the dynamic instability regions of a sandwich plate with a viscoelastic core, the dynamic instability analysis of plates with different values of α is performed. The results can be seen in Figure 4.12 which depicts the different dynamic instability principal regions. Table 4.6 presents the approximate values of the dynamic force and frequency of the cases loads on the minimum point of the principal dynamic instability's boundary for different α.

Table 4.6: Minimum of the dynamic instability principal region for different values of α

	P_d (N)	θ (rad/s)
$\alpha = 0$	0	3002.8
$\alpha = 5$	27.66	3003
$\alpha = 50$	276.3	3002
$\alpha = 100$	552.3	2999

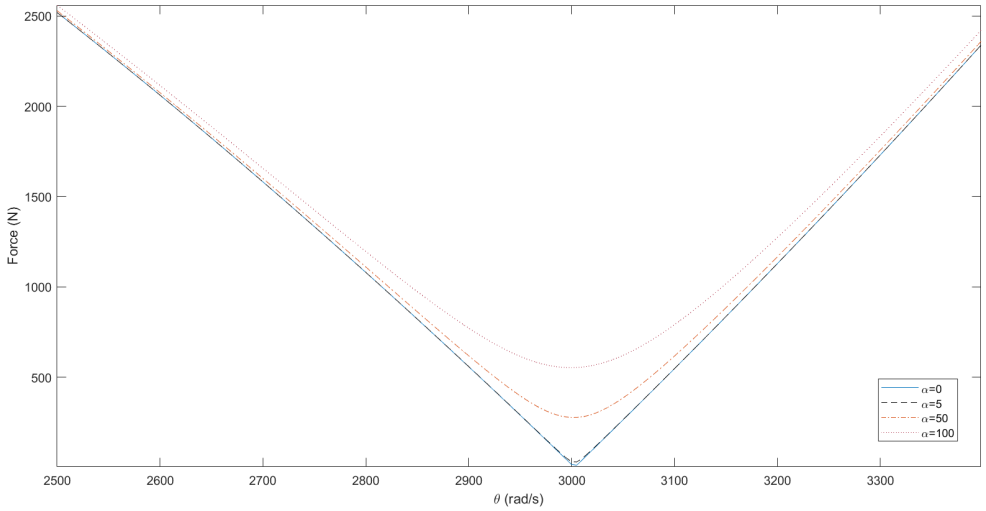

Figure 4.12: Principal dynamic instability region of a sandwich plate with viscoelastic core for different α

Hysteretic Damping

The dynamic stability analysis,using the hysteretic damping model, is performed on the sandwich plate with a viscoelastic core. The plate presents the same properties as the previous plate studied. Figure 4.13 depicts the principal dynamic instability region for a sandwich plate with $\eta = 0$, which would be equivalent to a sandwich plate with a purely elastic core. On the other side, Figure 4.14 presents the principal dynamic instability region for a sandwich plate with a viscoelastic core with $\eta = 0.1$.

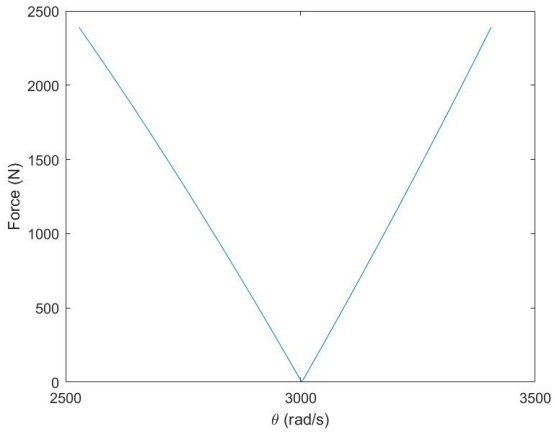

Figure 4.13: Principal dynamic instability region for $\eta = 0$

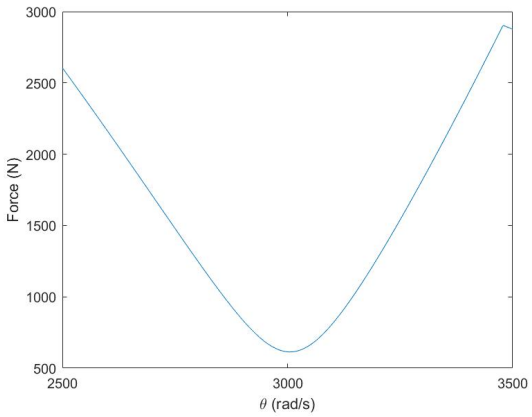

Figure 4.14: Principal dynamic instability region for $\eta = 0.10$

To analyse the effect of the variance of the core material loss factor η on the dynamic instability of the plate, Figure 4.15 depicts the principal dynamic instability region for multiple values of η. In Table 4.7 are shown the values of the dynamic force and frequency of the lowest point of the principal dynamic instability region's boundary for the different values of η.

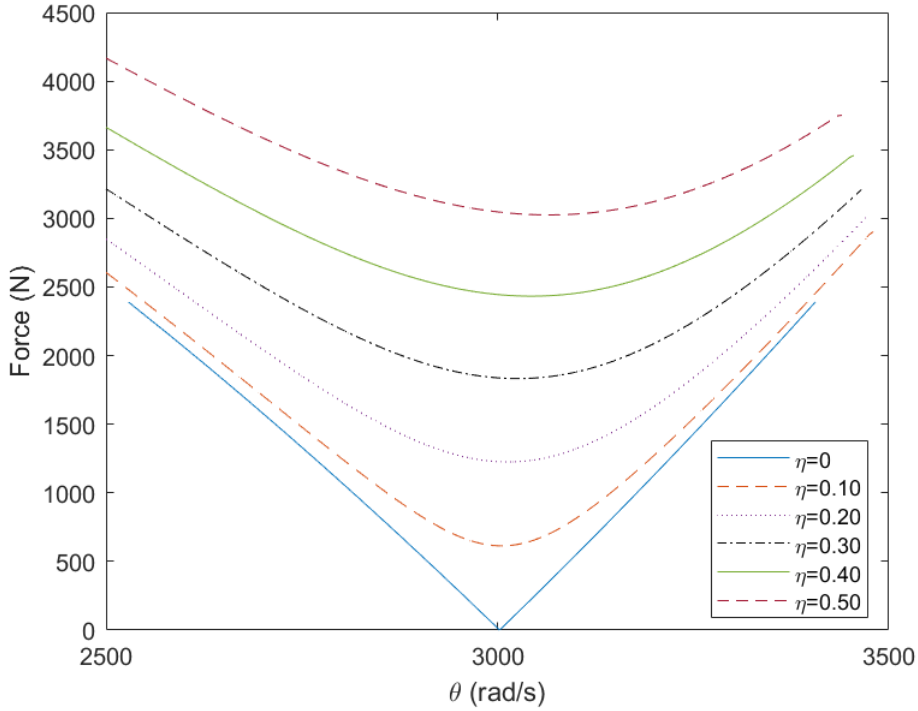

Figure 4.15: Principal dynamic instability region of a sandwich plate with viscoelastic core for different η

Table 4.7: Minimum of the dynamic instability principal region fo different values of η

	P_d (N)	θ (rad/s)
$\eta = 0$	0	3003
$\eta = 0.10$	613.8	3005
$\eta = 0.20$	1225	3013
$\eta = 0.30$	1833	3026
$\eta = 0.40$	2433	3043
$\eta = 0.50$	3025	3066

Conclusions

From the results presented, it is possible to conclude that adding a viscoelastic core to a sandwich plate will add damping to the system. Damping will transform the dynamic instability region. The minimum will present a round shape instead of a peak and that minimum is for any positive dynamic force applied to the system.

Besides that, Figures 4.10(a-d) and 4.11(a-d) allow to better understand the changes on the mechanical behaviour of the plate with viscoelastic core. These diagrams are also a good way to check the reliability of the regions obtained. Figures 4.10 depict the expected diagrams for a system with no damping where the points outside the dynamic instability region will show a stable behaviour in which the amplitude keeps the same over time, and the points inside the unstable region present an increase

of the amplitude with time. It is relevant to mention, that this increase becomes more sensitive when the point is further away from the boundaries. On the other side, Figures 4.11 depict a very different behaviour. Figures 4.11(a), 4.11(b) and 4.11(c) are characterised by a displacement function whose amplitude decreases exponentially with time. Since the point C' is in the boundary between regions or really close to it, it shows a softer damping where the decrease of amplitude is slower than the others. Figure 4.11(d) shows a typical unstable behaviour which was the expected result since point D' is in the unstable region.

Furthermore, the results obtained using proportional damping, and presented in Figure 4.12, show that the increase of α reduces the area of the unstable dynamic region. This area reduction is due to the fact that when α increases the minimum of the boundary is a load case with a higher dynamic force applied.

For the hysteretic damping the results obtained show the already expected change on the dynamic instability region and that as η increase the value of the force at the minimum also increases. Besides that, Table 4.7 shows that there is, also, a slow shift to the right of the principal dynamic instability region with the increase of η. It is possible to say that a viscoelastic core improves the dynamic behaviour of a sandwich plate since it reduces the area of its dynamic instability region.

Chapter 5

Conclusions

With all the work developed and presented, in this chapter a reflection of the results obtained and possible future developments and improvements on the area will be performed.

5.1 Achievements

The work developed in this thesis allowed to enlarge the computationally efficient finite element models already developed in Matlab by Tomé[32]. It added two more analyses, a free vibration analysis and a dynamic instability analysis, with and without damping.

Beginning with Chapter 2 *Development of Plates Elements*, the formulations used to model isotropic, orthotropic and laminated composite plates were presented. Besides that the mass matrix was created and added to the formulations. A free vibration analysis was performed to an isotropic and an orthotropic plate in order to validate the models developed.

Secondly, in Chapter 3 *Dynamic Instability Analysis* the numerical model used to study the dynamic instability of the structures analysed was developed. This model was applied to isotropic, orthotropic and laminated composite plates, whose results validated the model presented. Throughout this chapter, results from many studies were provided, showing how various parameters might affect the dynamic instability of the plates analysed. These parametric studies covered the changes in parameters like the ratios b/h and a/b.

Lastly, in Chapter 4 *Sandwich Plates* the formulations to model these plates were presented. The sandwich plate was simulated using the two theories and formulations discussed in Chapter 2, with the face sheets based on the FSDT and the core based on the HSDT. The model developed was first validated by a free vibration analysis. The strong agreement of the results obtained shows that the generated mass and stiffness matrices are being created as intended and producing decent outcomes. After the validation, the dynamic instability model, previously developed in Chapter 3, was applied to a sandwich plate. The results obtained validated, once again, the models used and that the generated Matlab code is working as planned and delivering satisfactory results. One more parametric study was performed. This time was to analyse the impact that the thickness of the core has on the dynamic

behaviour of the system.

At the end, in section 4.2, a viscoelastic material was used in the core of the sandwich plate which added damping to the system. Two different models to add the damping to the system were developed, one as proportional damping and the other as hysteretic damping. Even though it was not possible to validate these results due to the scarce literature on this topic, the results obtained were in accordance with what was expected.

5.2 Future Work

Developments and extensions of the present work can be done through multiple ways. Some relevant ideas, but not exclusively, are:

- The work can be extended adding piezoelectric sensors and actuators to the model and studied their effect on the dynamic instability;
- Validation of the results obtained in the present work through experimental studies;

Adding Piezoelectric Sensors and Actuators

One interesting development is adding, on the top and bottom surfaces of the sandwich plate, symmetric piezoelectric sensors and actuators patches and analyse how it would behave. The computational model developed was adapted from one previous used to study the buckling and static behaviour of a sandwich plate with piezoelectric patches, which means that the adaption would be achieved easily with just a few adjustments on the computational process. Study the effect of the patches on the dynamic instability regions would be useful to apply them in order to achieve better and more effective structures to use it in a more wide range of applications and industries. Besides that, a lot of studies can be done using the piezoelectric effect. Multiple control feedback laws can be used and each one of them would affect the plate behaviour in a different way.

Experimental Studies

One important future work would be experimental studies of the results obtained in this work. Although this would involve some investment due to the equipment and materials needed to do so, it would be interesting and important for the sake of better understanding the behaviour of sandwich plates. It would allow to understand if the numerical models present some kind of errors or deviation and would help to find solutions to improve them in order to better use composite plates in different applications.

These are just some ideas of possible future studies of sandwich plates, but a lot more can be done. It is always important to think that, the better this kind of structure is studied and its behaviour is known, the better it can be applied in different applications and its unexpected failure can be prevented.

Bibliography

[1] C. A. Osheku. *Lamination*. IntechOpen, Mar 2018. ISBN 978-953-51-3926-3.

[2] A. Krzyzak, M. Mazur, M. Gajewski, K. Drozd, A. Komorek, and P. Przybyłek. Sandwich structured composites for aeronautics: Methods of manufacturing affecting some mechanical properties. *International Journal of Aerospace Engineering*, 2016, 2016. doi: 10.1155/2016/7816912.

[3] M. Kheirikhah, S. Khalili, and K. Malekzadeh Fard. Biaxial buckling analysis of soft-core composite sandwich plates using improved high-order theory. *European Journal of Mechanics - A/Solids*, 31 (1):54–66, 2012. doi: https://doi.org/10.1016/j.euromechsol.2011.07.003.

[4] M. Shariyat. A generalized high-order global–local plate theory for nonlinear bendingand buckling analyses of imperfect sandwich plates subjectedto thermo-mechanical loads. *Composite Structures*, 2009.

[5] A. Tian, R. Ye, and Y. Chen. A new higher order analysis model for sandwich plates with flexible core. *Journal of Composite Materials*, 50:949–961, 3 2016. doi: 10.1177/0021998315584650.

[6] The vertical stabilizer - aeroclass.org. URL `https://www.aeroclass.org/vertical-stabilizer/`. Last accessed on: 2022-08-30.

[7] Iate a motor serenity mia da benetti é vendido - boat shopping. URL `https://www.boatshopping.com.br/mercado-global/iate-a-motor-serenity-mia-da-benetti-e-vendido/`. Last accessed on: 2022-08-30.

[8] Y. Xiao, Y. Hu, J. Zhang, C. Song, X. Huang, J. Yu, and Z. Liu. The bending responses of sandwich panels with aluminium honeycomb core and cfrp skins used in electric vehicle body. *Advances in Materials Science and Engineering*, 2018, 08 2018. doi: 10.1155/2018/5750607.

[9] M. R. PERMOON and T. FARSADI. Free vibration of three-layer sandwich plate with viscoelastic core modelled with fractional theory. *Mechanics Research Communications*, 116, 2021. doi: https://doi.org/10.1016/j.mechrescom.2021.103766.

[10] S. S. Rezvani and M. S. Kiasat. Analytical and experimental investigation on the free vibration of a floating composite sandwich plate having viscoelastic core. *Archives of Civil and Mechanical Engineering*, 18(4):1241–1258, 2018. doi: https://doi.org/10.1016/j.acme.2018.03.006.

[11] L. S. Ramachandra and S. K. Panda. Dynamic instability of composite plates subjected to non-uniform in-plane loads. *Journal of Sound and Vibration*, 331:53–65, 1 2012. doi: 10.1016/j.jsv.2011.08.010.

[12] L. Briseghella, C. Majorana, and C. Pellegrino. Dynamic stability of elastic structures: a finite element approach. *Computers Structures*, 69(1):11–25, 1998. doi: https://doi.org/10.1016/S0045-7949(98)00084-4.

[13] V. V. Bolotin. *The Dynamic Stability of Elastic Systems*. HOLDEN-DA Y, INC., 1964.

[14] I. Mascolo. Recent developments in the dynamic stability of elastic structures. *Frontiers in Applied Mathematics and Statistics*, 5, 10 2019. doi: 10.3389/fams.2019.00051.

[15] S. Wang and D. Dawe. Dynamic instability of composite laminated rectangular plates and prismatic plate structures. *Computer Methods in Applied Mechanics and Engineering*, 191(17), 2002. doi: https://doi.org/10.1016/S0045-7825(01)00354-1.

[16] W.-R. Chen, C.-S. Chen, and J.-H. Shyu. Stability of parametric vibrations of laminated composite plates. *Applied Mathematics and Computation*, 223:127–138, 2013. doi: https://doi.org/10.1016/j.amc.2013.07.095.

[17] M. Loja, J. Barbosa, and C. Mota Soares. Dynamic instability of variable stiffness composite plates. *Composite Structures*, 182:402–411, 2017. doi: https://doi.org/10.1016/j.compstruct.2017.09.046.

[18] M. Loja and J. Barbosa. In-plane functionally graded plates: A study on the free vibration and dynamic instability behaviours. *Composite Structures*, 237:111905, 2020. doi: https://doi.org/10.1016/j.compstruct.2020.111905.

[19] M. Darabi and R. Ganesan. Nonlinear dynamic instability analysis of laminated composite thin plates subjected to periodic in-plane loads. *Nonlinear Dynamics*, 91:187–215, 1 2018. doi: 10.1007/s11071-017-3863-9.

[20] M. Darabi and R. Ganesan. Non-linear vibration and dynamic instability of internally-thickness-tapered composite plates under parametric excitation. *Composite Structures*, 176:82–104, 2017. doi: https://doi.org/10.1016/j.compstruct.2017.04.059.

[21] D. R. Reddy, B. S. Ratnam, and G. V. Rao. Prediction of dynamic stability behavior of thin square plates subjected to constant compressive and periodic including constant compressive loads on perpendicular edges. *International Journal of Current Engineering and Technology*, 2:620–624, 1 2013. doi: 10.14741/ijcet/spl.2.2014.118.

[22] S. Mondal and L. Ramachandra. Dynamic instability of damped composite plates with embedded delaminations. *Journal of Sound and Vibration*, 455:221–240, 2019. doi: https://doi.org/10.1016/j.jsv.2019.05.014.

[23] A. Nayak, S. Moy, and R. Shenoi. Free vibration analysis of composite sandwich plates based on reddy's higher-order theory. *Composites Part B: Engineering*, 33(7):505–519, 2002. doi: https://doi.org/10.1016/S1359-8368(02)00035-5.

[24] J.-Y. Kao, C.-S. Chen, and W.-R. Chen. Parametric vibration responde of foam-filled sandwich plates under periodic loads. *Mech Compos Mater*, 48:525–538, 2012. doi: https://doi.org/10.1007/s11029-012-9297-z.

[25] A. Sankar, S. Natarajan, and M. Ganapathi. Dynamic instability analysis of sandwich plates with cnt reinforced facesheets. *Composite Structures*, 146:187–200, 2016. doi: https://doi.org/10.1016/j.compstruct.2016.03.026.

[26] R. Sahoo and B. N. Singh. Dynamic instability of laminated-composite and sandwich plates using a new inverse trigonometric zigzag theory. *Journal of Vibration and Acoustics, Transactions of the ASME*, 137, 12 2015. doi: 10.1115/1.4030716.

[27] R. Sahoo and B. N. Singh. Dynamic instability of laminated composite and sandwich plates using a new inverse hyperbolic zigzag theory. *Journal of Aerospace Engineering*, 28, 7 2015. doi: 10.1061/(asce)as.1943-5525.0000440.

[28] S. V. Joseph and S. C. Mohanty. Free vibration and parametric instability of viscoelastic sandwich plates with functionally graded material constraining layer. *Acta Mechanica*, 230:2783–2798, 8 2019. doi: 10.1007/s00707-019-02433-8.

[29] R. K. Ojha and S. K. Dwivedy. Parametric instability analysis of sandwich plates with composite skins and lpre based viscoelastic core. *Journal of Sandwich Structures and Materials*, 23:3685–3716, 11 2021. doi: 10.1177/1099636220942472.

[30] D. Li. Layerwise theories of laminated composite structures and their applications: A review. *Archives of Computational Methods in Engineering*, 28:577–600, 3 2021. doi: 10.1007/s11831-019-09392-2.

[31] R. Moreira and J. Dias Rodrigues. A layerwise model for thin soft core sandwich plates. *Computers Structures*, 84(19):1256–1263, 2006. doi: https://doi.org/10.1016/j.compstruc.2006.01.020. Computational Models for Multilayered Structures and Composite Structures.

[32] M. F. A. Tomé. Buckling analysis of laminated composite and sandwich plates considering the piezoelectric effect. Master's thesis, Instituto Superior Técnico, October 2021.

[33] A. Araújo, V. Carvalho, C. Mota Soares, J. Belinha, and A. Ferreira. Vibration analysis of laminated soft core sandwich plates with piezoelectric sensors and actuators. *Composite Structures*, 151:91–98, 2016. doi: https://doi.org/10.1016/j.compstruct.2016.03.013.

[34] J. N. Reddy. *Mechanics of laminated composite plates and shells : theory and analysis*. Boca Raton : CRC Press, 2nd edition, 2004.

[35] M. Abbas, M. Elshafei, and H. Negm. Modeling and analysis of laminated composite plate using modified higher order shear deformation theory. *International Conference on Aerospace Sciences and Aviation Technology*, 15:1–25, 2013. doi: 10.21608/asat.2013.22182.